NUREG/CR-3546
MEA-2030

The Temperature Dependence of Fatigue Crack Growth Rates of A 351 CF8A Cast Stainless Steel in LWR Environment

Prepared by W. H. Cullen, R. E. Taylor, K. Torronen, M. Kemppainen

Materials Engineering Associates, Inc.

Prepared for
U.S. Nuclear Regulatory Commission

GPO Printed copy price: $3.75

NUREG/CR-3546
MEA-2030
RF, R5

The Temperature Dependence of Fatigue Crack Growth Rates of A 351 CF8A Cast Stainless Steel in LWR Environment

Manuscript Completed: February 1984
Date Published: April 1984

Prepared by
W. H. Cullen, R. E. Taylor, K. Torronen*, M. Kemppainen*

Materials Engineering Associates, Inc.
9700-B George Palmer Highway
Lanham, MD 20706

*Technical Research Centre of Finland

Prepared for
Division of Engineering Technology
Office of Nuclear Regulatory Research
U.S. Nuclear Regulatory Commission
Washington, D.C. 20555
NRC FIN B8133

ABSTRACT

The fatigue crack growth rates for A 351-CF8A cast stainless steel were determined over a range of temperatures from 95°C to 338°C (200°F to 640°F). The waveform was 17 mHz sinusoidal and the load ratio was 0.2. The environment was borated and lithiated water with a dissolved oxygen content of ~ 1 ppb. The results show an easily measurable (factors of 2 to 8) increase in crack growth rates due to the environment. However, these rates are well within the known band of results for low-alloy pressure vessel and low-carbon piping steels in LWR environments. An extensive fractographic investigation shows fatigue fracture surfaces covered with brittle-like features. This morphology is similar to that resulting from the environmental assistance mechanism producing increased crack growth rates due to stress-corrosion cracking.

CONTENTS

LIST OF FIGURES

Figure Page

ACKNOWLEDGEMENT

The author would like to acknowledge the efforts of Craig Miller (of ENSA) for assistance in conducting this research effort. Appreciation is also extended to Frank J. Loss, who provided program management during this research effort. The continuing support and encouragement of the NRC Project Manager, M. Vagins, has been appreciated.

1. INTRODUCTION

Of the ten standardized compositions of heat-and corrosion-resistant cast Fe-Cr, Fe-Cr-Ni or Ni-base alloys, only two , A 217 and A 351 , are intended for pressure containment applications. This report describes fatigue crack growth rates in one of these , A 351 - CF8A. The basic ASTM standard A 351 is a generic specification for a wide range of compositions of high alloy cast stainless steels. The suffix, CF8A, describes more particularly the nature of the particular alloy. The first letter, either C or H, designates the Corrosion or Heat-resistant quality of the alloy. The second letter designates the chromium and nickel range; the letters progress from A to Z as the nickel increases. In particular, the F designation represents the 20% chromium and 10% nickel composition. The one or two digit numeral which follows specifies the maximum carbon content for the alloy , 0.8% in this case. The final letter(s) describes special alloying additions or characteristics of the casting process. In this particular case, the A indicates heats of steel in which the Cr:Ni ratio is increased within the allowable limits, giving a higher delta ferrite content, and a higher strength.

The composition of the alloy examined in this case is given in Table 1. It has been recognized that some compositions in this "F" category, specifically those with higher chromium, 21% to 23%, and lower nickel, 7.5% to 8.5%, will be characterized by a rather large percentage of ferrite in the microstructure, and this leads to a long-term low temperature aging or sensitization problem in this series of alloys. Elements which promote ferrite formation, such as silicon, molybdenum or columbium (niobium) will aggravate the aging phenomenon. Manganese, nitrogen and carbon tend to promote austenite and thus offset the embrittlement tendency. The chemical analysis of this steel results in a delta ferrite content of 17.4%, which is below the range of values (25% to 40%) at which aging is a demonstrated problem. The microstructure of the heat of steel described in Table 1 is shown in Fig. 1.

Either 25 mm or 50 mm thick compact specimens (1T-CT or 2T-CT) were cut from the shell of a research pressure vessel which was about 700 mm in inside diameter, with 65 mm thick walls. Specimens were aligned with the crack propagation direction parallel to either the axial or circumferential direction as noted in the discussion. Tests were conducted in simulated PWR coolant, with a nominal chemistry as given in Table 2.

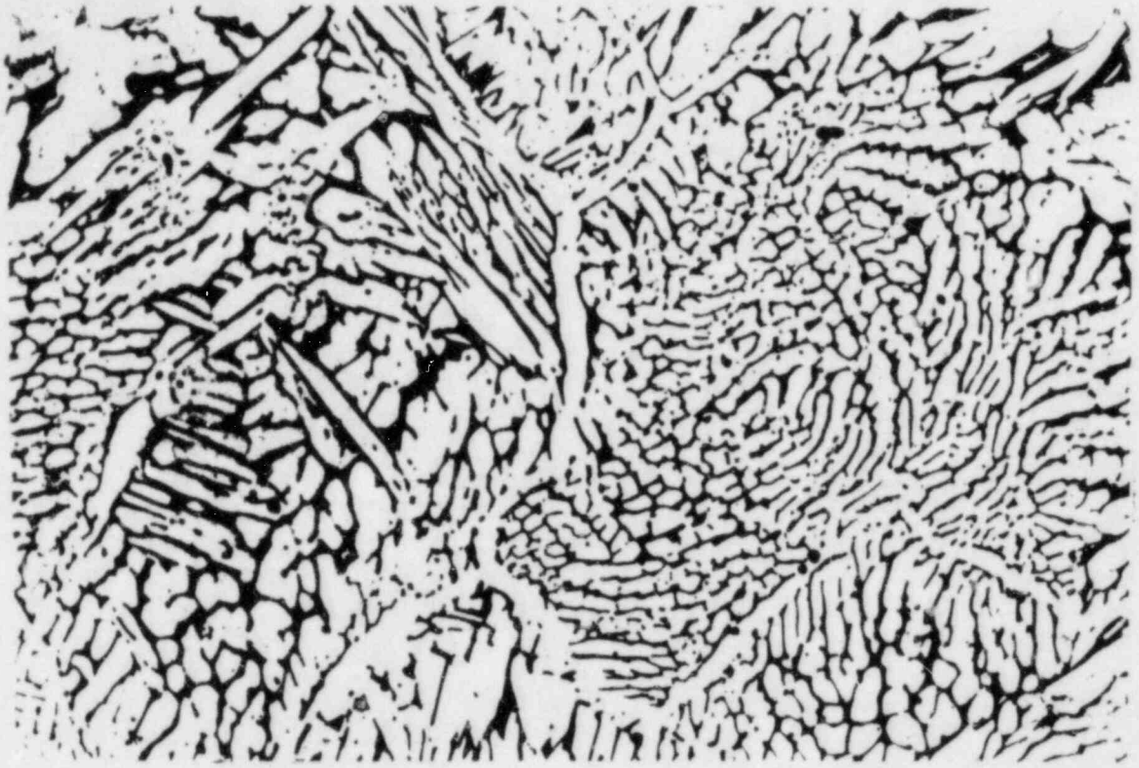

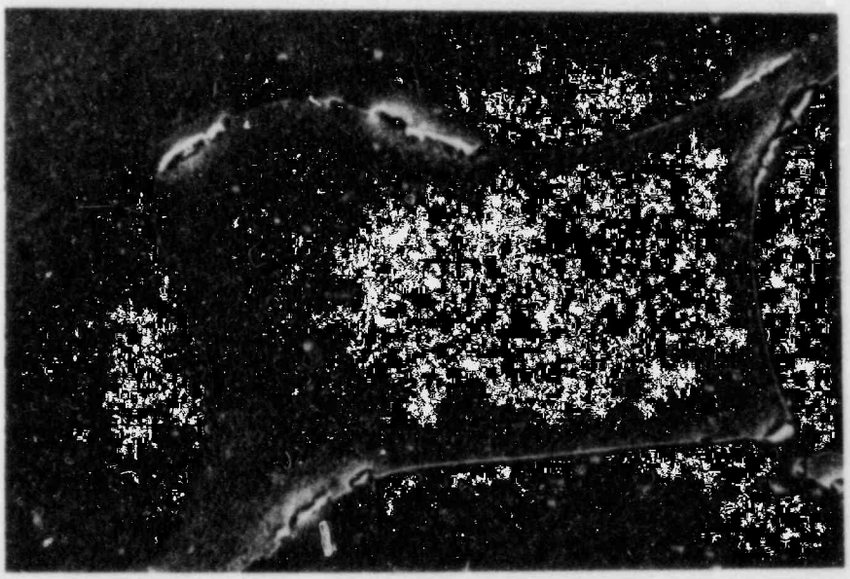

Fig. 1. The microstructure of the steel described in Table 1, showing (a) an optical micrograph of austenite dendrites in a matrix of delta ferrite and (b) an electron mic ograph of precipitated carbides on the austenite-ferrite phase boundary.

Table 1. Chemical composition and mechanical properties of the alloy used in this study.

Chemical Analysis, %		Mechanical Tests, Transverse
0.06	Carbon	At Room Temperature:
0.68	Manganese	
1.17	Silicon	Yield Strength, 0.2% offset 303 MPa (43,950 psi)
20.42	Chromium	
8.58	Nickel	Tensile Strength, 560 MPa (81,250 psi)
0.07	Cobalt	Elongation, in 51 mm (2 in.) 48%
0.020	Phosphorus	
0.018	Sulphur	At 650°F:
17.4	Delta Ferrite	Yield Strength, 0.2% offset 159 MPa (23,100 psi)

Table 2. Chemistry of the simulated PWR coolant used in this study

Boron (as boric acid)	1000 ppm
Lithium (as lithium hydroxide)	1 ppm
Chloride ions	<0.15 ppm
Fluoride ions	<0.10 ppm
Dissolved oxygen	~ 1 ppb
Dissolved hydrogen (saturation)	30-50 cm^3/kg water

Note: All other metallic or ionic species should be at about trace levels. Some iron, both in solid and soluble form is the inevitable result of a corroding specimen.

2. EXPERIMENTAL PROCEDURES

The hardware and general procedures used in these tests was generally described in Ref. 1. In the four years since that reference was published, several improvements have been made, and this report presents an opportunity to discuss all of these changes.

2.1 Test Facilities

The test facilities remain essentially unchanged from the description given in Ref. 2. Since the publication of that reference, the single specimen autoclaves were installed in hot cells and were used in the testing of several irradiated specimens of pressure vessel steels (Ref. 3). Subsequently, they were relocated and reinstalled at the Nuclear Science and Technology Facility in Buffalo, NY, and are currently in use. In both cases, extensive replumbing of the water circulation loops was accomplished. The low-temperature test chamber (<100°C (<212°F)), and the multispecimen test chambers (MTS #1, #2 and #3) were reinstalled in the Materials Engineering Associates laboratory in Lanham, and at that time were upgraded by addition of a new pressure pump and an improved plumbing scheme. Subsequently, the #3 unit was further upgraded to operate at the higher pressure and temperature required for the 338°C (640°F) tests as part of the present study. Additionally, a high-pressure, high temperature circulation pump became available, and one of these was installed on unit #2. The basic components of the current system are shown in Fig. 2.

2.2 Crack Length Measurement

2.2.1 Measurement Methodology

Very few changes have been made to the basic evaluation of crack length using the computer technique as described in Ref. 4. The computerized data acquisition system computes current crack length at specific cyclic intervals by recording 100 pairs of crack mouth opening (CMO) and applied load (P) readings during the rising load part of the cycle. The crack length is then calculated from a formula of the form

$$a = f\left(\frac{\alpha E B\,(CMO)}{P}\right)$$

in which a is crack length, B is specimen thickness, E is the elastic modulus, and the function f is dependent on specimen geometry. The use and significance of the correction factor (α) is given in Section 2.2.3. While some laboratories have adopted a procedure which specifies data acquisition during the decreasing load part of the cycle, there should

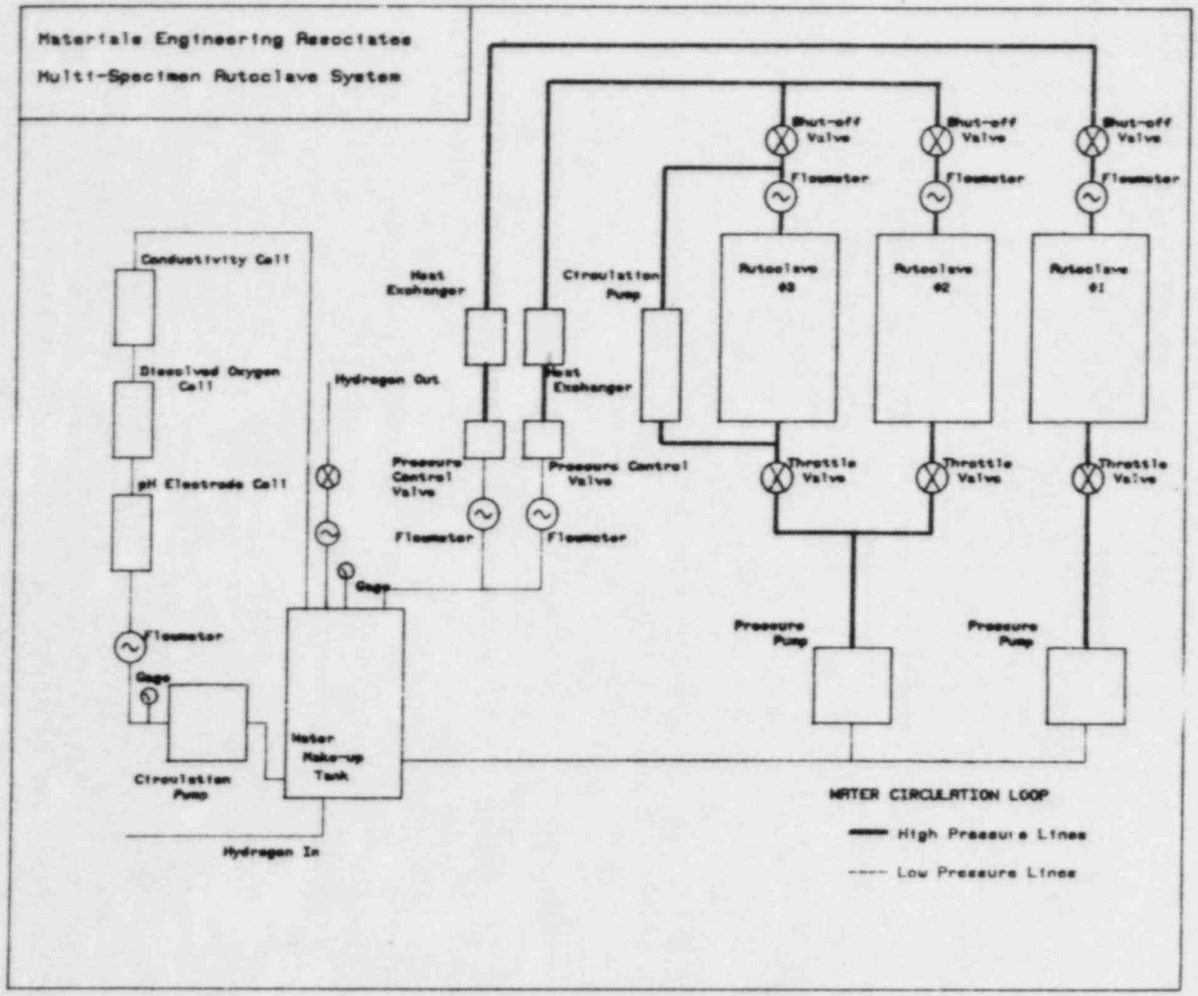

Fig. 2. Schematic of water circulation loop for three-autoclave test facility.

be no intrinsic difference between the two, assuming measurable crack extension does not occur during the cycle and the specimen response is purely elastic. Each CMO and P data pair is actually the average of four CMO and three P readings, which are interlaced (CMO-P-CMO-P, etc.); the system requires about four milliseconds to take these readings. This digital averaging procedure greatly improves the signal-to-noise ratio in the acquired data, and results in a much higher correlation coefficient for the linear fit of the CMO vs. P data set. Independent crack length readings are taken for three successive cycles, and are averaged, providing further resolution of the crack length calculation. For each specimen under test, the previous five readings are used to make a rough evaluation of the current crack growth rate, and this is used to "predict" when the next reading should be scheduled. This provides for constantly decreasing cyclic intervals between readings, as the crack growth rate steadily increases over the course of each test.

2.2.2 Techniques for Multiple Specimen Testing

The 100 liter autoclaves normally contain four 50 mm thick compact (CT) or wedge opening loaded (WOL) specimens. These are often four different steels, different crack orientations from the same heat, or a combination of the two. The specimens are notched and precracked to a/W ratios of ~0.35 to 0.40. The specimens are installed in the autoclave, which is then sealed and filled with water mixed to the nominal PWR chemistry shown in Table 2. The water is heated under ambient pressure to about 95°C (203 °F) to drive out the dissolved oxygen and held for 10-15 hours. Since the water expands as the temperature increases from ambient to 95°C, the top overflow valve is left open to allow the excess volume of water and the effervesced oxygen to drain away. The autoclave is then sealed, pressurized and the temperature brought to the desired set point. The water continues to deoxygenate by passing through a pressure regulation valve, and circulating to the feedwater tank, which is continuously purged with flowing hydrogen while an equivalent amount of thoroughly deoxygenated water is pumped to pressure and flows to the autoclave. In this way the last few parts per billion of dissolved oxygen are removed and the entire system (the most recently loaded autoclave as well as others on line) settles to the operating level of 0 to 2 ppb dissolved oxygen.

Each test begins by fatigue cracking the specimens about 2 to 4 mm using a 1 Hz sinusoidal waveform and the test loads which are desired. The purpose of this is twofold. First, it brings the cracks closer to an a/W ratio of about 0.5 and a regime in which the compliance to crack length function has a significantly greater slope than for shorter cracks (say a/W = 0.3). This results in greater accuracy in determining crack extension. Secondly, this procedure should result in significant "pumping" of the environment, and in time, should assist in establishing a steady-state electrochemical condition near the crack tip. This latter point has not been proven, since that would require crack enclave measurements which are not possible at this time.

When any one of the four specimens has achieved ~4 mm of extension at 1 Hz, the cycling is stopped, and the function generators are adjusted

to the desired test frequency and waveform combination; we have used 17 mHz sinusoidal in this program. The test is then restarted. In the usual case, one specimen will arrive at the desired terminal crack length before the others. No specimen is allowed to fail unstably, since the final crack length must be beachmarked for the purposes of post-test correction. Thus, when one specimen does reach the terminal crack length, the test is interrupted, the loads are reduced 50% to 60% and the test frequency and waveform are changed to 1 Hz sinusoidal. The daisy chain is then fatigued to allow that longest crack to grow through the specimen, leaving a clear beachmark indicating the position and curvature of the crack front at the end of the test for that specimen. Crack growth in the remaining specimens is usually slight, but is carefully monitored during this phase.

When failure of the first specimen is complete, the loads and test frequency and waveform are returned to their desired values, and testing resumes on the remaining three specimens. As before, one of the remaining three specimens progresses more rapidly to the terminal crack length and the above reduced load/increased frequency procedure is repeated. When the second specimen is adequately beachmarked, the test resumes on the third and fourth remaining specimens. After the third specimen reaches the desired terminal crack length, and is also beachmarked, the test continues on the final specimen until it reaches its terminal length and the test is stopped.

At this point the autoclave is cooled to a few degrees below the boiling point and the water is dumped while the specimens are still warm. This assists in the rapid evaporation of water from the specimens and helps eliminate oxidation (rusting) which would confuse subsequent oxide analysis of the fatigue fracture surfaces. The autoclave is unsealed, and the specimens are removed and broken open to reveal the fatigue fracture surface.

The above procedure results in specimens which are beachmarked between one and three times, with concurrent crack extension ranging from essentially zero up to several millimeters. Table 3 gives a summary of a typical set of crack extensions for an autoclave loading involving some of the results for this test series. We have completed testing several autoclave loadings using this beachmarking procedure, and have concluded that this does not introduce significant transients in the fatigue crack growth behavior. This is best demonstrated by examination of plots of crack growth rate vs. crack length, shown in Figs. 3 and 4. These data sets correspond to specimens indicated in Table 3. In each case, fatigue crack growth rates resumed the same trend before and after each beachmarking incident. Photographs of two of these specimens are shown in Fig. 5. The beachmarks resulting from changes in load or frequency are visible, especially on the smoother fatigue surface of the low-carbon steel, F0P-89.

2.2.3 Pre- and Post-Test Corrections

At the inception of any test, the experimentalist approximates the notch length of a precracked specimen on the basis of the crack length measured at the surface. At the beginning of each test, once at temperature, our

Table 3. Multispecimen Test History - Autoclave #3 - 338°C (640°F)

Specimen I.D.	Begin[a] 1	End 1	End 2	End 3	End 4	End 5	End 6	End 7	End 8
A9-107	50.5	53.0	70.5	74.7					
A9-110	48.9	50.7	62.33	62.9	67.3	71.5			
FOP-89	49.8	53.6	59.4	60.7	62.8	65.4	71.1		
FOP-90	50.2	53.4	57.5	57.5	58.5	58.7	59.8	60.0	72
∞	1 Hz fatigue precrack in water environment	17 mHz test on all specimens	1 Hz beachmark on A9-107. Some growth on FOP-89. No growth on FOP-90	17 mHz test on three specimen remaining A9-107 breaks somewhere in this interval	1 Hz beachmark on A9-110. Some growth on the remaining two specimens	Continue 17 mHz test on two FOP specimens	1 Hz to break FOP-89. Some growth on FOP-90	Continue last phase of 17 mHz test on FOP-90	Stop Test
Cycle Count	0	28199	77260	93638	102007	166565	175874	288319	327180
Day	1	1	34	36	43	44	51	53	81

[a] Begin/End refer to the phase of the test sequence through which a particular frequency and load combination are used. Phases 1, 3, 5 and 7 consisted of 1 Hz sinusoidal cycling, phases 2, 4, 6 and 8, 17 mHz sinusoidal cycling.

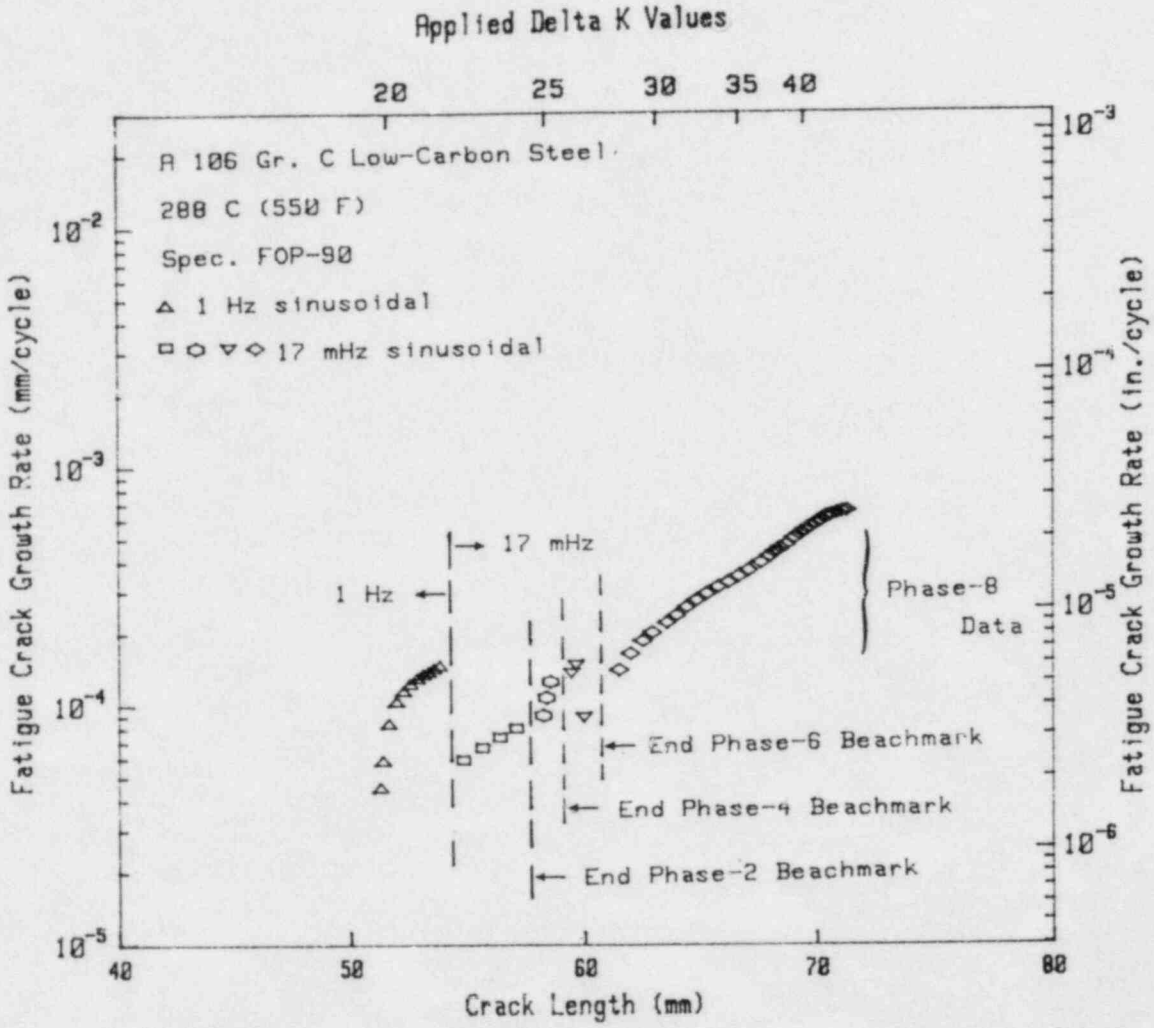

Fig. 3. Fatigue crack growth rate vs. crack length, showing insensitivity of growth rate to interruptions for beach marking. Data for the various phases are shown in Table 3.

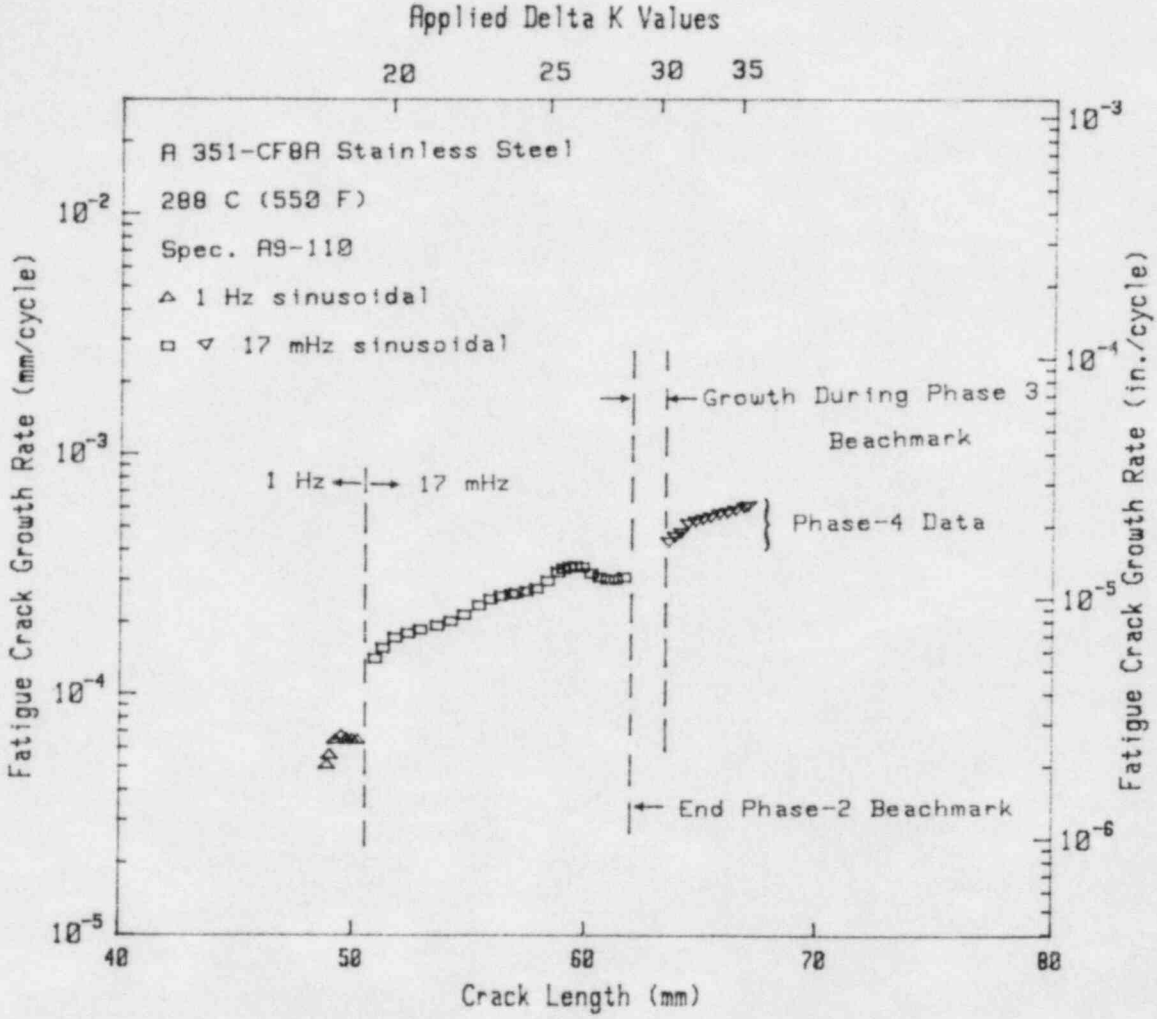

Fig. 4. Fatigue crack growth rate vs. crack length, showing insensitivity of growth rate to interruptions for beach marking. Data for the various phases are shown in Table 3.

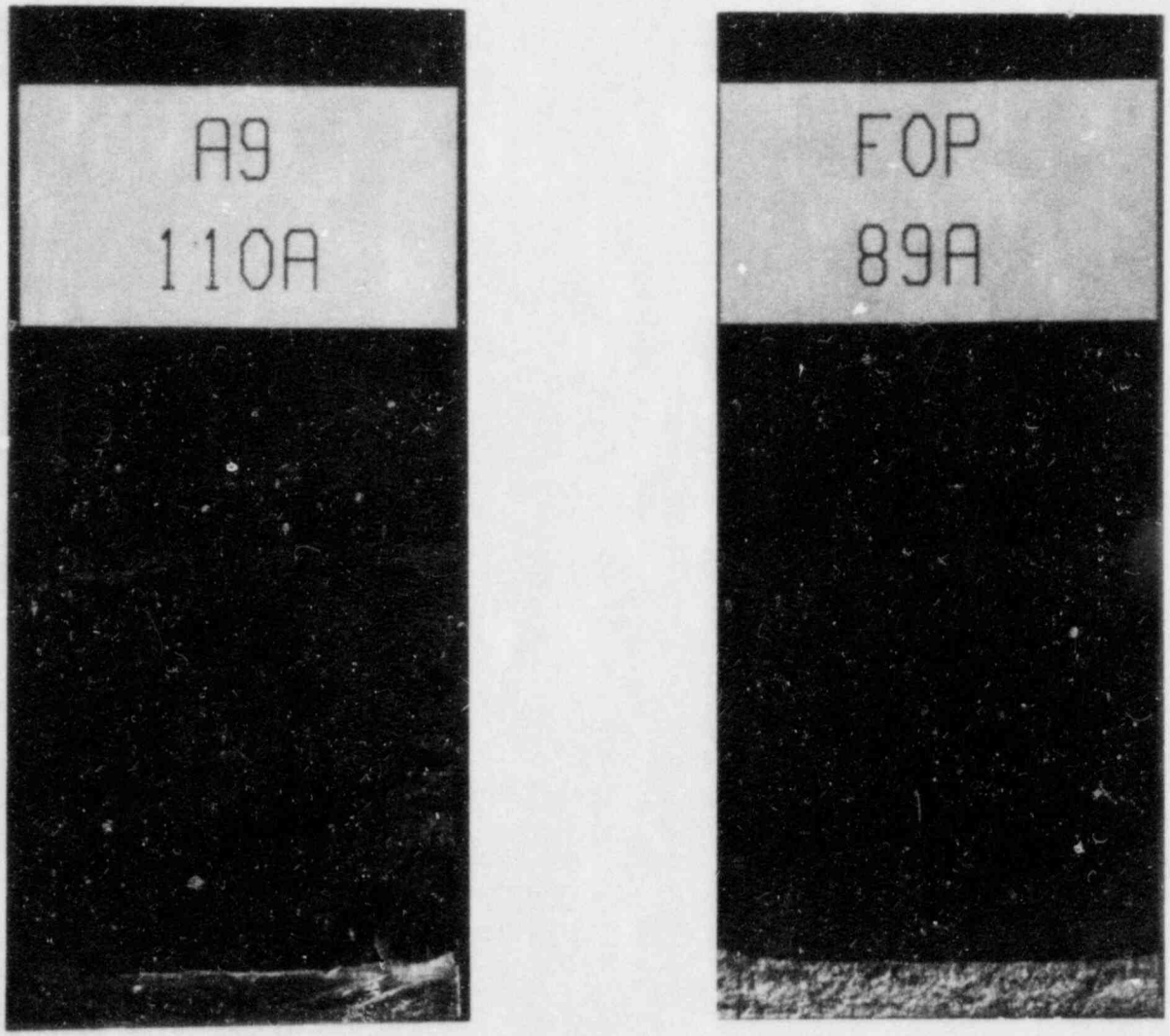

Fig. 5. Two specimens from the autoclave loading described in Sec. 2.2.2. The beachmarks are distinguished more clearly on FOP-89A.

general procedure is to "force" the first computer-acquired and processed data point to be equal to this approximate crack length. This is computationally accomplished by adjusting the factor $\alpha(=1)$ in the equation for crack length,

$$a = f\left(\alpha \frac{EB\delta}{P}\right) \qquad (1)$$

thus, if B, δ, P and a (corrected for tunneling) are accurately known, and $\alpha = 1$, then E should be the actual elastic modulus for the material. However, the elastic modulus is not known for every heat of material tested, and an approximate value is often used. Other small system-related errors, such as aging-induced calibration errors in the displacement gage, or changes in gain of the load and displacement transducer conditioners may affect unnoticeably the factors in the compliance equation over a period of time. Thus the α factor, when properly adjusted, makes up for these accumulated errors or inaccuracies. In practice, α is combined with the raw data for B, E, and P, and is varied, to the fifth significant digit, until the correct initial crack length is computationally generated. The α-factor thus becomes a way of simultaneously correcting for variances in any of the variables in the compliance equation. This fitted α-factor is then used in every application of Eq. 1 during the balance of the test.

It must be pointed out that this method corrects only for errors in the computation of crack length. While within the context of the crack length equation, it does account for variance in load cell calibration, along with all the other variances of the compliance-determination "system", it does not account for a load cell calibration error by itself. Hence, errors in the load cell calibration factor, whether intrinsic to it, or whether occuring during a test, will still be directly reflected as uncorrected errors in ΔK, and will result in erroneous shifts in the data on a da/dN vs. ΔK plot. Frequent checks of the load cell calibration are the only assurance that this error will be minimized.

Specimens are usually chilled in liquid nitrogen and broken open, leaving sharply defined profiles of the intermediate and final cracks which can be easily measured. In spite of the surface-oxidation caused by the high-temperature, aqueous environment used in this research, the precrack front and beach marks caused by the load and frequency changes, are visible and measurable. Each of these crack fronts should be measured using the five-point method included in ASTM-E647 (Ref. 5). The differences between the optically-measured crack fronts, and the corresponding α-adjusted, compliance-inferred crack lengths is termed the crack length correction. In the ideal case of no error, this amounts to a correction only for curvature, which is not measurable from the surface trace of the precrack, and which may change during the course of a test, and therefore E647 refers to a "crack curvature correction."

The curvature correction described in E647 is to be applied linearly with respect to crack length, using the customary "lever law" type of proration. When a compliance technique is being used, a different method of correction should be applied. In essence, a correction factor (α_1) is derived to

correct the compliance values for the initial crack length error and curvature combined, and a second correction factor (α_2) is derived, to correct the compliance values for the error and curvature correction to the final crack length or beach-marked interval. The list of compliance values for all data points is then corrected, using a separate α value for each point obtained by linearly scaling between α_1, and α_2 against cyclic count, N. This amounts to scaling against time, since the underlying assumption is that errors accruing in crack length are due to time-wise drift in the displacement gage or load cell conditioner circuits, or elsewhere in the analog instrumentation associated with the compliance measurement system. In the ideal case $\alpha_1 = \alpha_2$, indicating that the curvature remained constant throughout the test, and that no errors accrued in the measurement systems.

It is the authors' recommendation that this correction method be applied in every case, regardless of the 5% criteria of E647. Physically, this procedure provides exact matches of the initial and final crack lengths, and accurately corrects for all intermediate crack lengths assuming only time-wise, linearly-accruing errors in gage or load cell calibration. The procedure is shown schematically in Fig. 6.

It should be obvious that there could be case-by-case adjustments to the above procedure. For example, if the specimen fracture surface contains a non-deliberate beachmark which also can be accurately related to a cyclic count value, then the above procedure can be broken into two parts: a complete correction from precrack to beach mark, and a second complete correction from beach mark to final.

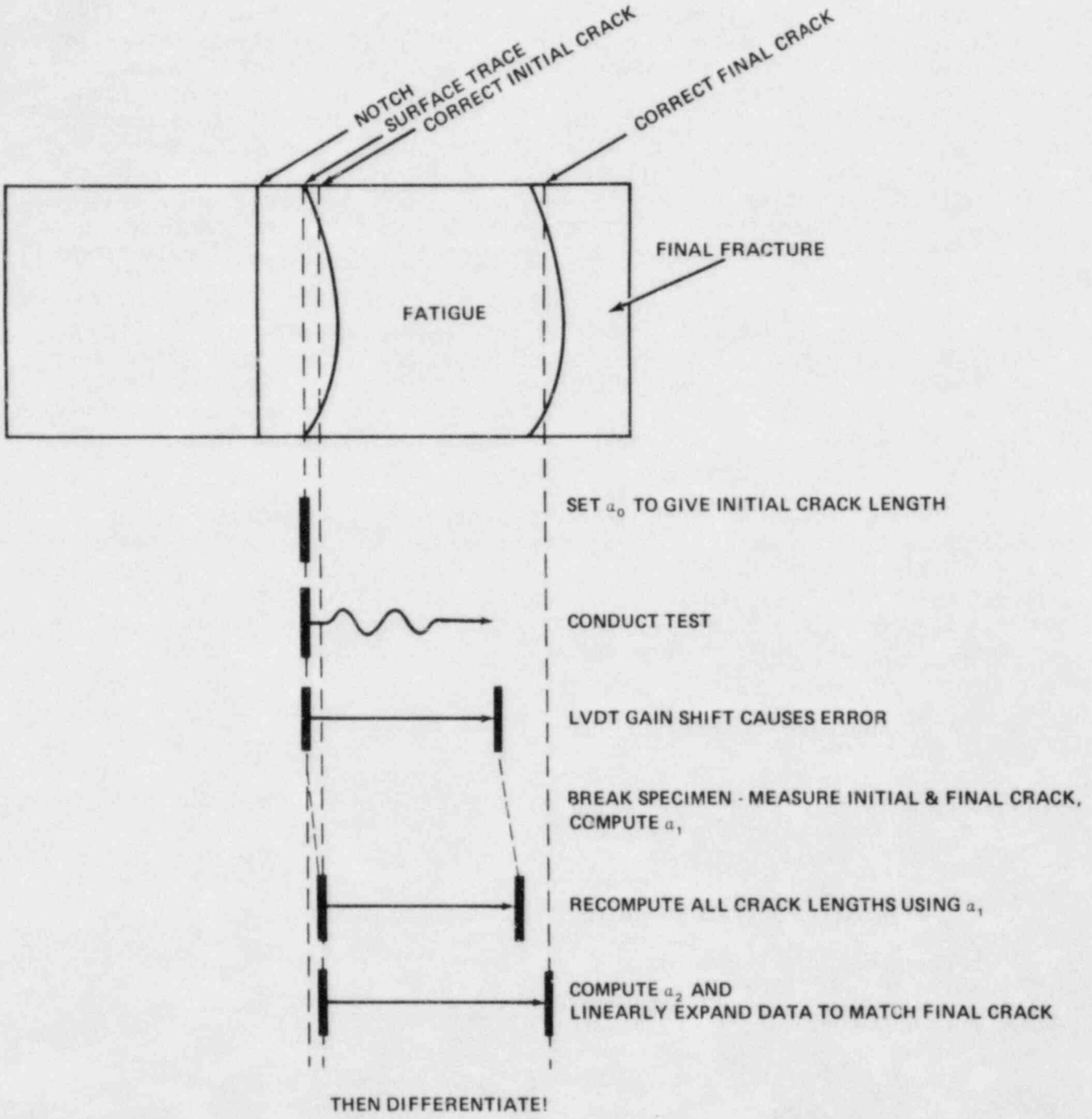

Fig. 6. A schematic illustration of the computation and application of α-factors to produce corrected crack lengths on examination of the fatigue fracture surface.

3. RESULTS AND DISCUSSION

3.1 Crack Growth Rate Results

Fatigue crack growth rate studies on this class of materials (CF8, CF8A and CF8M) have been conducted by several authors. James has extensively investigated growth rates in air environment for CF8 and CF8M over a wide range of temperatures, at R values of 0.05 or 0.1. (Ref. 6). Bamford has published data for two load ratios, R=0.2 and 0.7, and frequencies of 170, 340 and 1000 mHz in a PWR environment (Ref. 7). The Bamford data show little environmental effect, presumably because of the rather high test frequencies. More recently, Amzallag, Bernard and colleagues have begun publishing results from an extended program to study aging effects in some of the higher ferrite casts (Ref. 8, 9). Some initial results, presented in August, 1983, show a factor of three elevation in growth rates for aged materials in a PWR environment (Ref. 10).

The results from the present investigation are shown in Figs. 7 through 11. In the latter three cases (T = 232°C, 288°C and 338°C) the growth rates for two orientations, axial and circumferential, are shown in separate panels, however, the differences between the results due to orientation at any of the three temperatures are undetectible. Overall, the lowest growth rates are for the intermediate temperatures of 232°C and 288°C, with the rates increasing moderately with both increasing and decreasing temperature. Each set of data, except the set for 177°C, shows a slight plateau behavior, although there appears to be no particular pattern to the ΔK range or da/dN range over which the plateaus extend. In all cases, the data sets reside well below the ASME Section XI, Appendix A reference lines (Ref. 11) for crack growth in pressure vessel steels; the reader should bear in mind that the Section XI reference lines apply only to carbon and low-alloy ferritic steels. However, the available data from this study and Ref. 8, 9 and 10, indicate that stainless steels also reside below the ASME reference lines. This suggests that they also could be considered as candidates for inclusion in the Section XI scheme.

The reader should note that the crack growth rates in these steels are comparable to those for ferritic pressure vessel and piping steels, particularly those with lower sulfur content (Ref. 12). For these stainless steels, the ΔK range over which rates are measured is foreshortened becasue they do not have sufficient flow stress to maintain the constraint necessary to satisfy the ASTM E 647 validity requirements. However, the growth rates show about the same dependence on ΔK, and a small "plateau" is developed at ΔK values of about 25 MPa $\sqrt{m}$. There is little measurable orientation dependence.

3.2 Fractographic Results

Macrophotographs of several of the specimens tested are shown in Figs. 5, 12a and 12b. Viewed optically, the fatigue fracture surfaces are rough, reflecting the influence of the large austenite grain size. The crack front

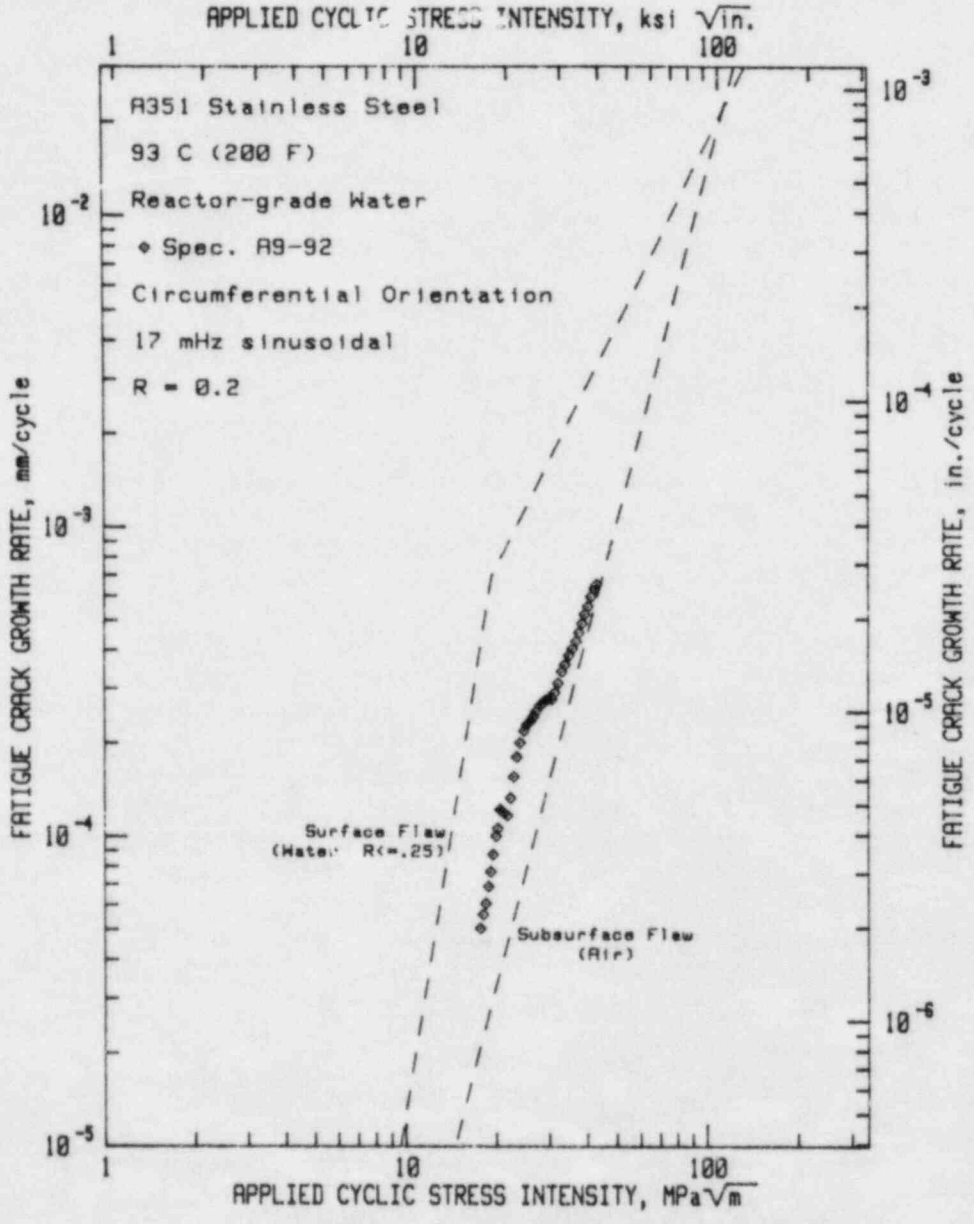

Fig. 7. Fatigue crack growth rates vs. applied ΔK for A 351-CF8A cast stainless steel, tested at R=0.2, 17 mHz sinusoidal waveform and a temperature of 93°C (200°F). The dotted lines are taken from Section XI of the ASME Boiler and Pressure Vessel Code (Ref. 11).

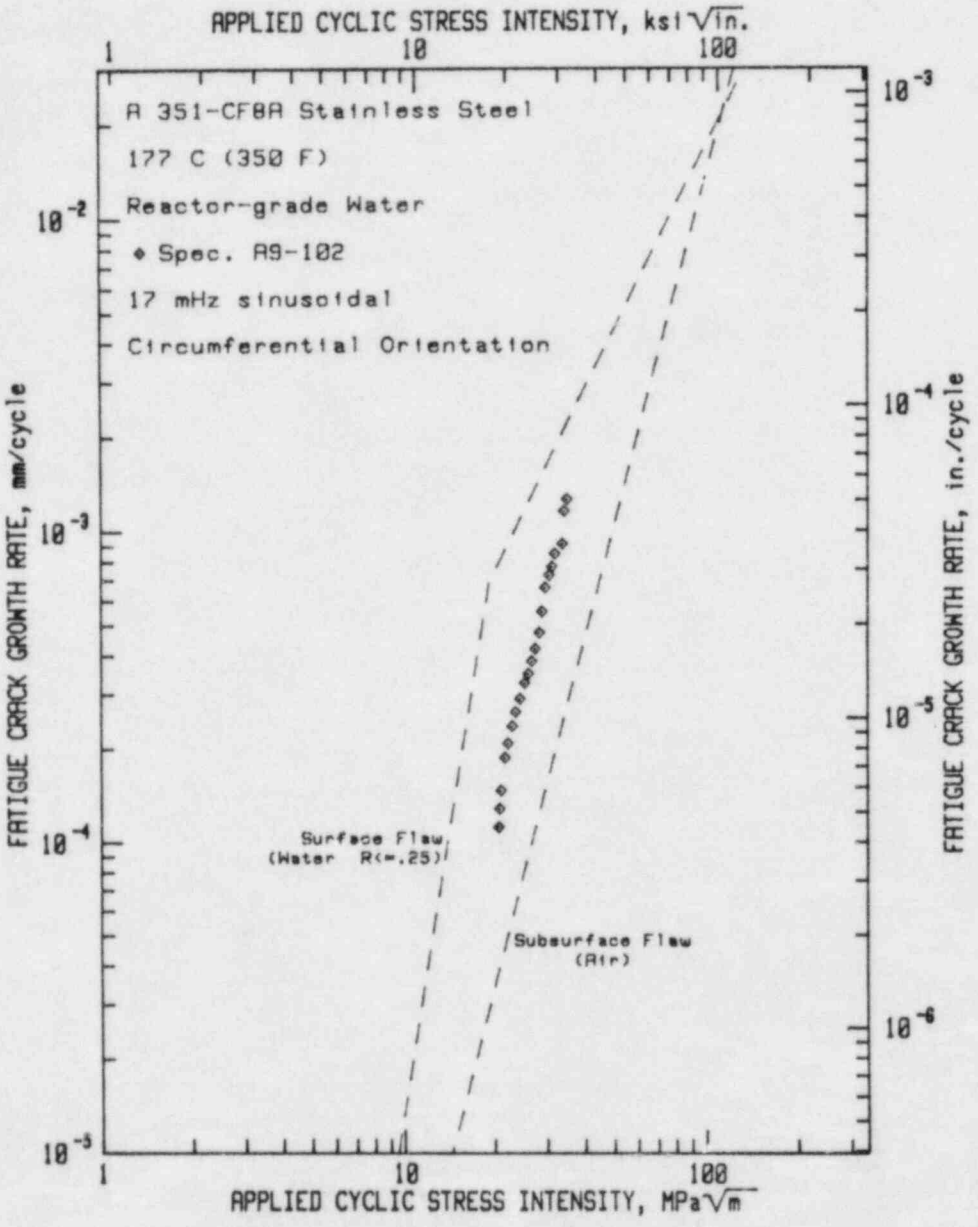

Fig. 8. Fatigue crack growth rates vs. applied ΔK for A 351-CF8A cast stainless steel, tested at R=0.2, 17 mHz sinusoidal waveform and a temperature of 177°C (350°F).

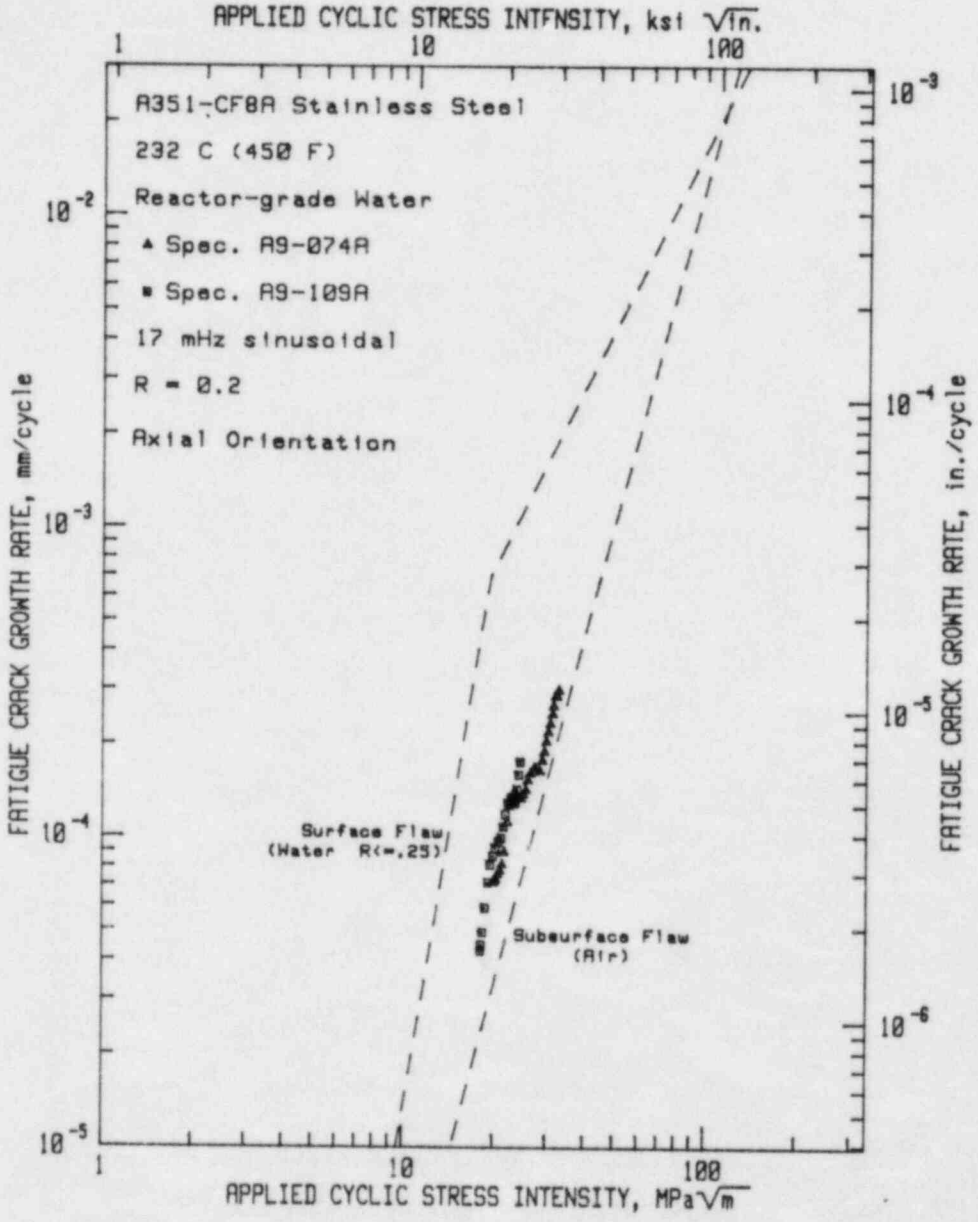

Fig. 9a. Fatigue crack growth rates vs. applied ΔK for A 351-CF8A cast stainless steel with the crack running in the axial direction. Test parameters were R=0.2, 17 mHz sinusoidal waveform and a temperature of 232°C (450°F).

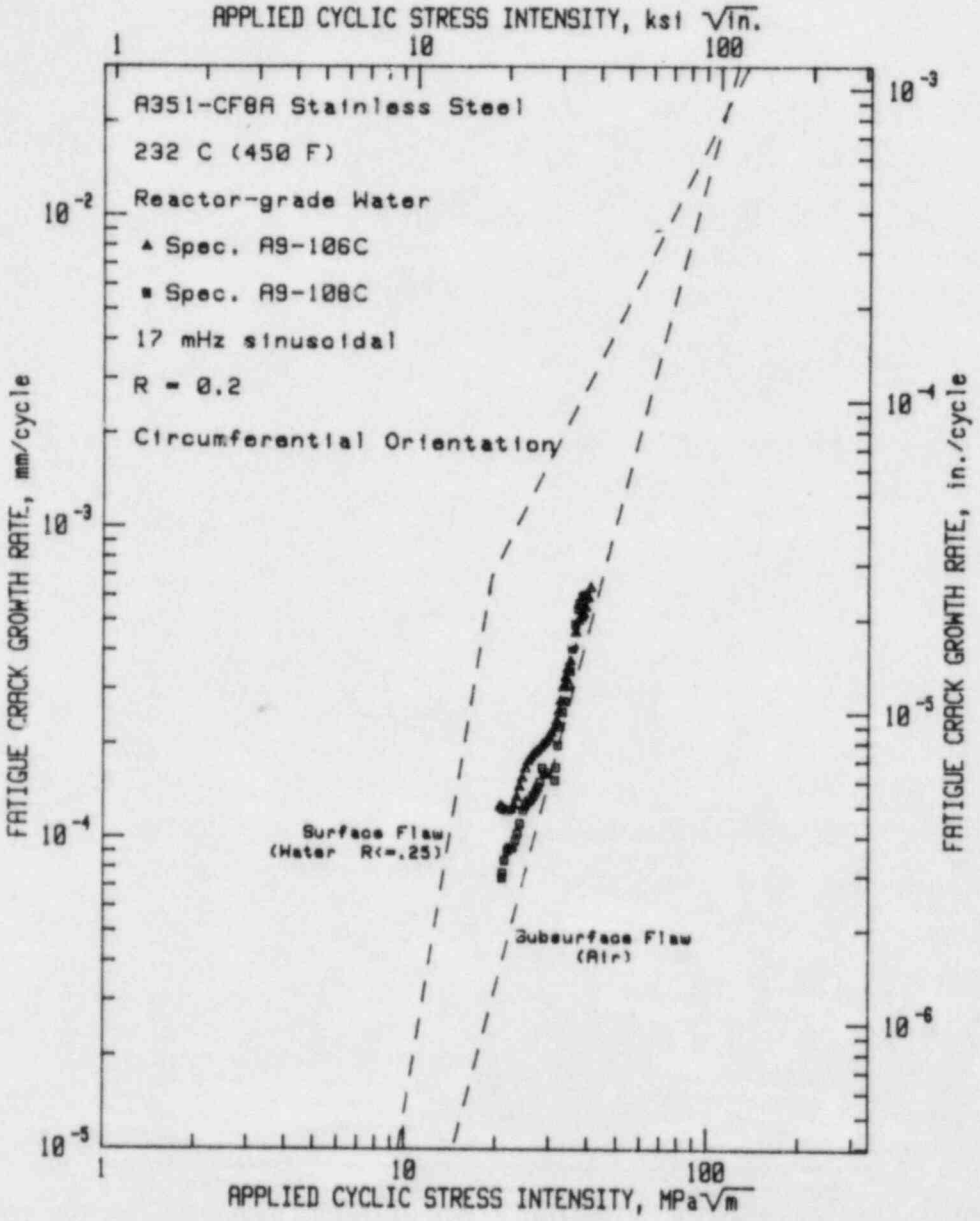

Fig. 9b. Fatigue crack growth rates vs. applied ΔK for A 351-CF8A cast stainless steel with the crack running in the circumferential direction. Test parameters were R=0.2, 17 mHz sinusoidal waveform and a temperature of 232°C (450°F).

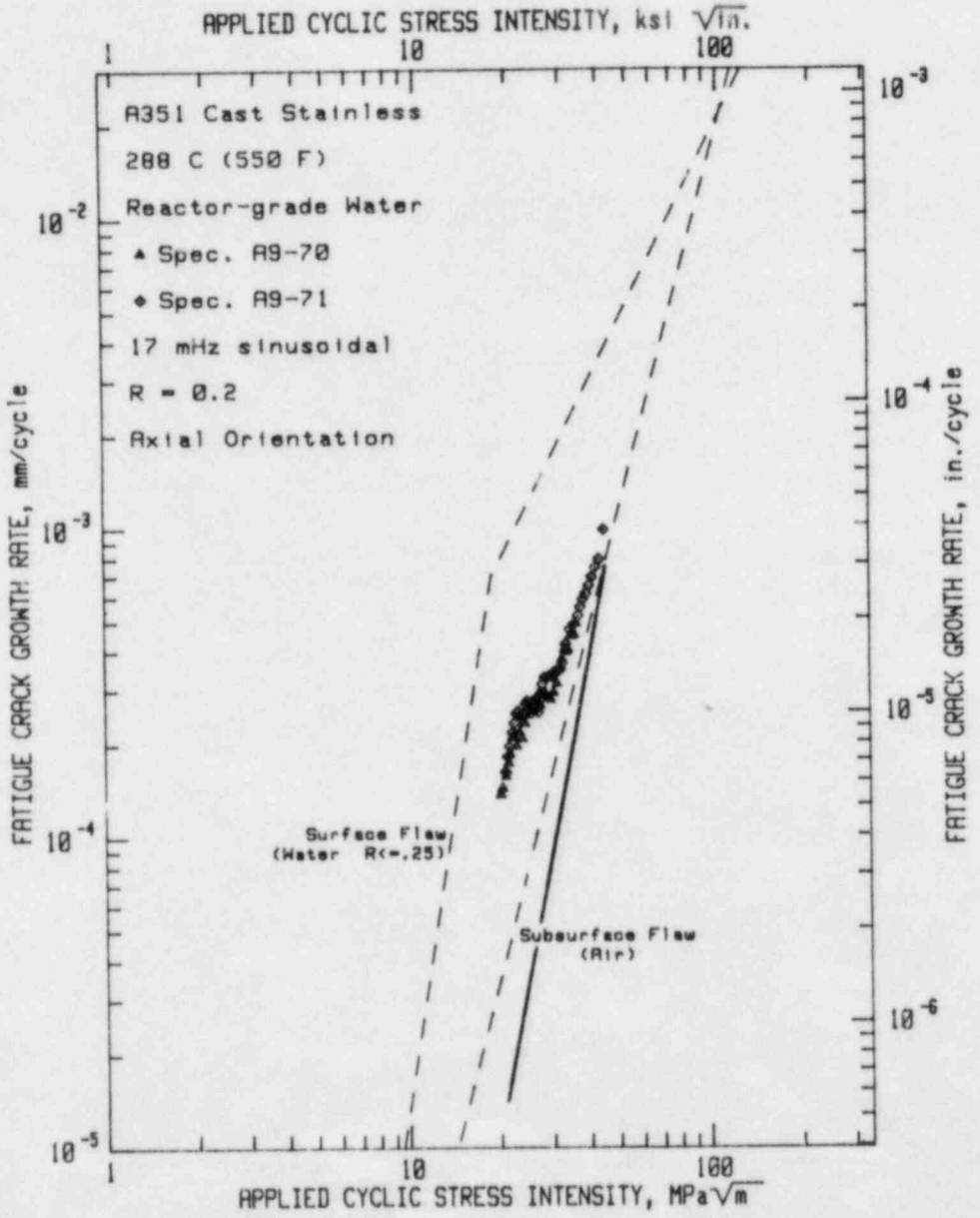

Fig. 10a. Fatigue crack growth rates vs. applied ΔK for A 351-CF8A cast stainless steel with the crack running in the axial direction. Test parameters were R=0.2, 17 mHz sinusoidal waveform and a temperature of 288°C (550°F). The solid line here and in Figs. 10b, 11a, and 11b, represents a best fit to the collection of air environment data for temperatures in the 288°C to 315°C (550°F to 600°F) range (Ref. 6).

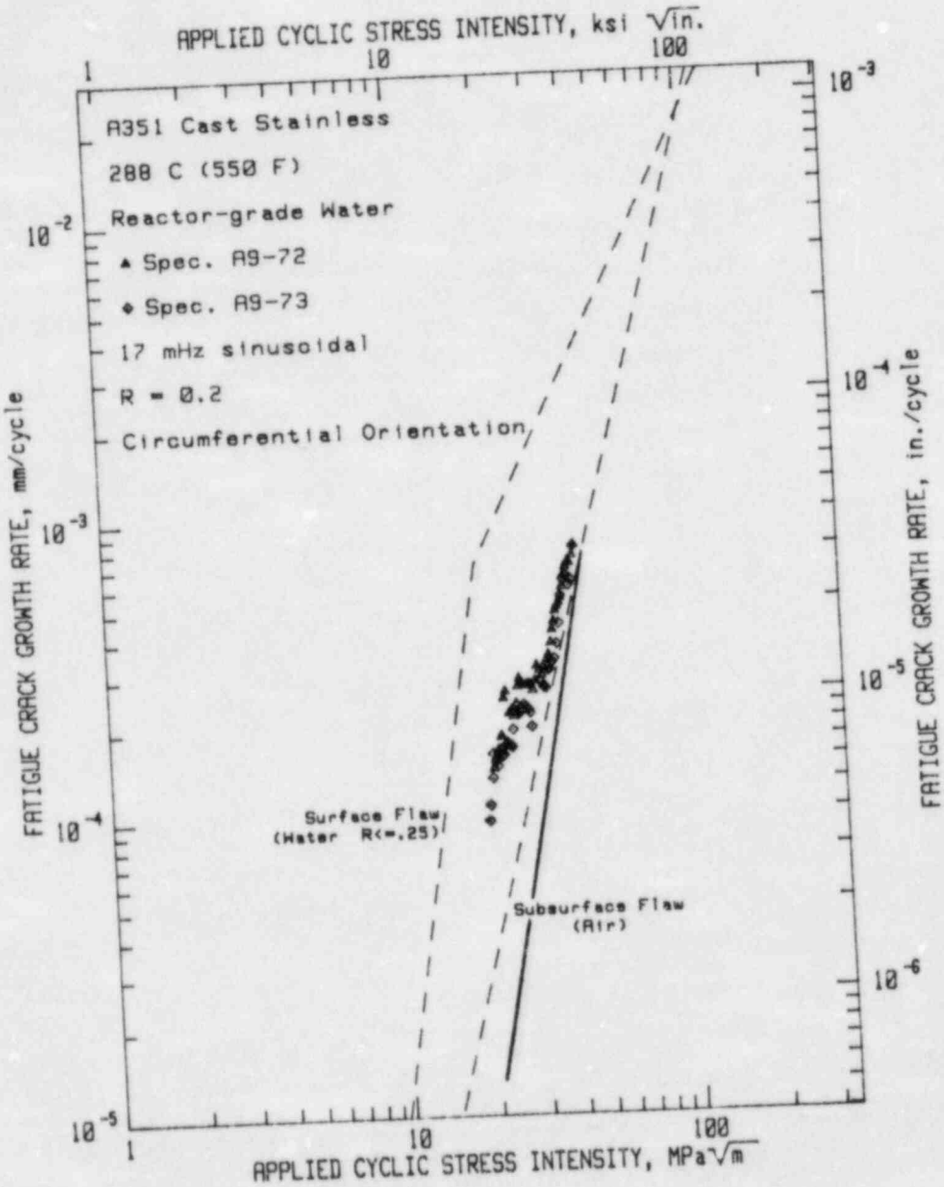

Fig. 10b. Fatigue crack growth rates vs. applied ΔK for A 351-CF8A cast stainless steel with the crack running in the circumferential direction. Test parameters were R=0.2, 17 mHz sinusoidal waveform and a temperature of 288°C (550°F).

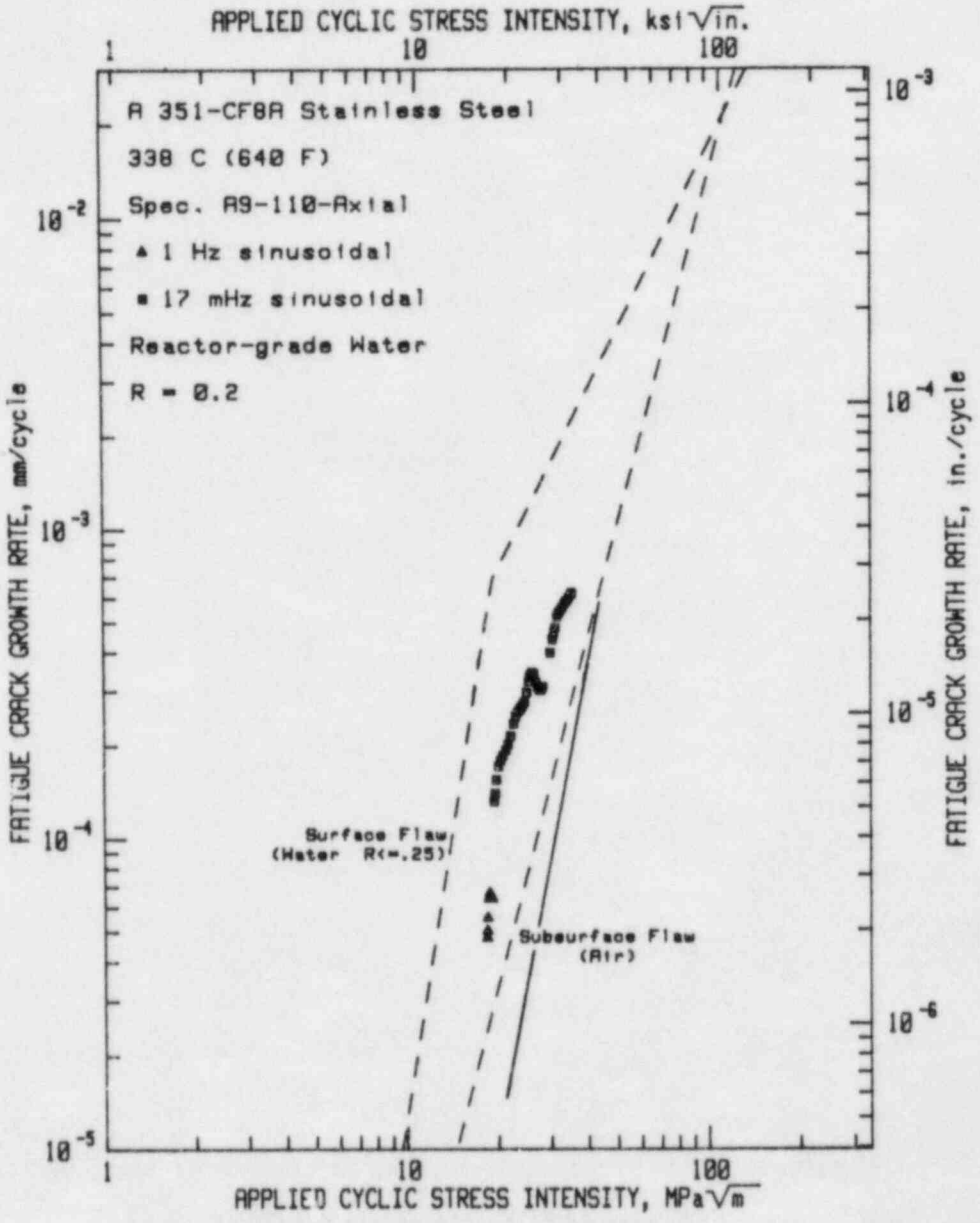

Fig. 11a. Fatigue crack growth rates vs. applied ΔK for A 351-CF8A cast stainless steel with the crack running in the axial direction. Test parameters were R=0.2, 17 mHz sinusoidal waveform and a temperature of 338°C (640°F).

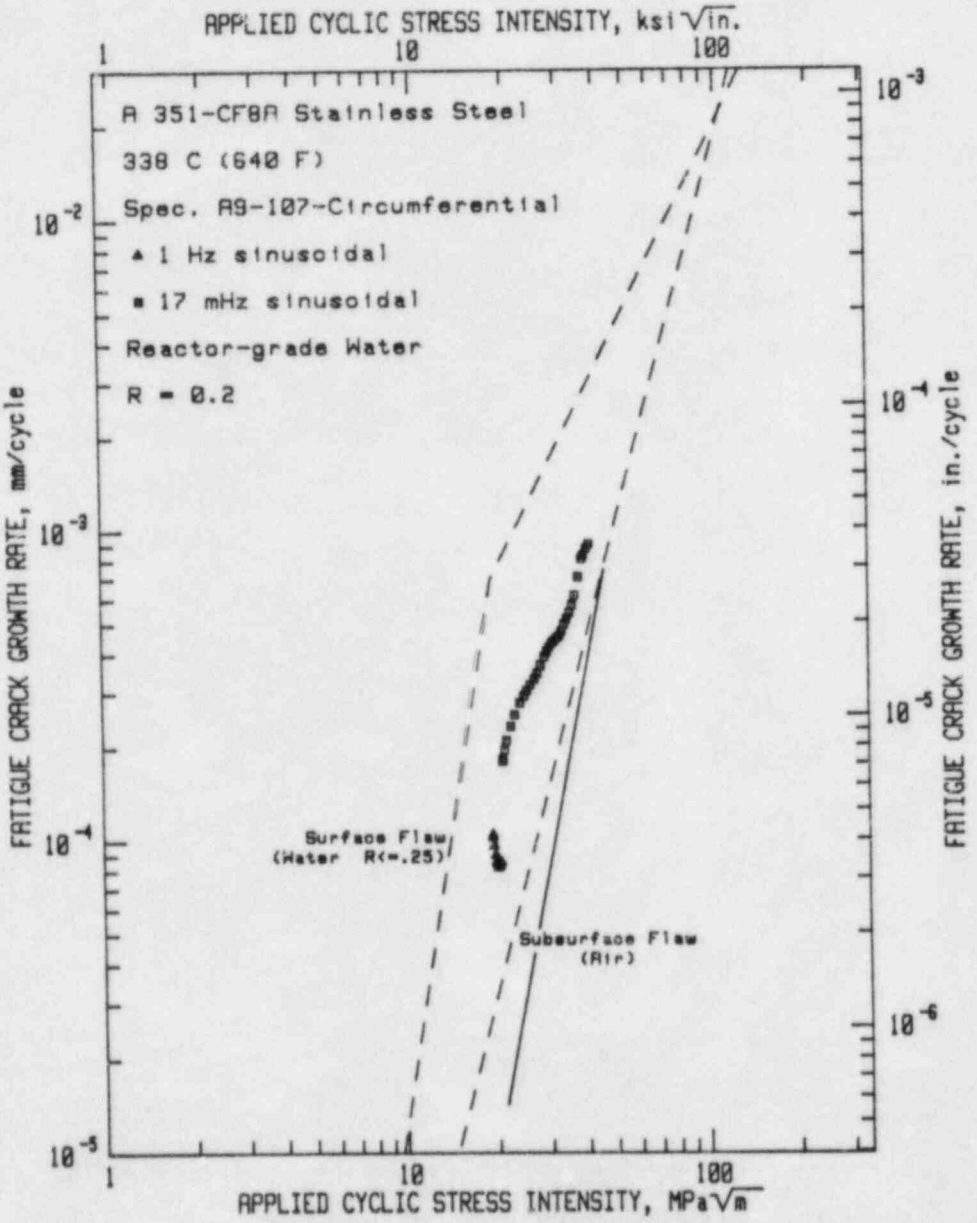

Fig. 11b. Fatigue crack growth rates vs. applied ΔK for A 351-CF8A cast stainless steel with the crack running in the circumferential direction. Test parameters were R=0.2, 17 mHz sinusoidal waveform and a temperature of 338°C (640°F).

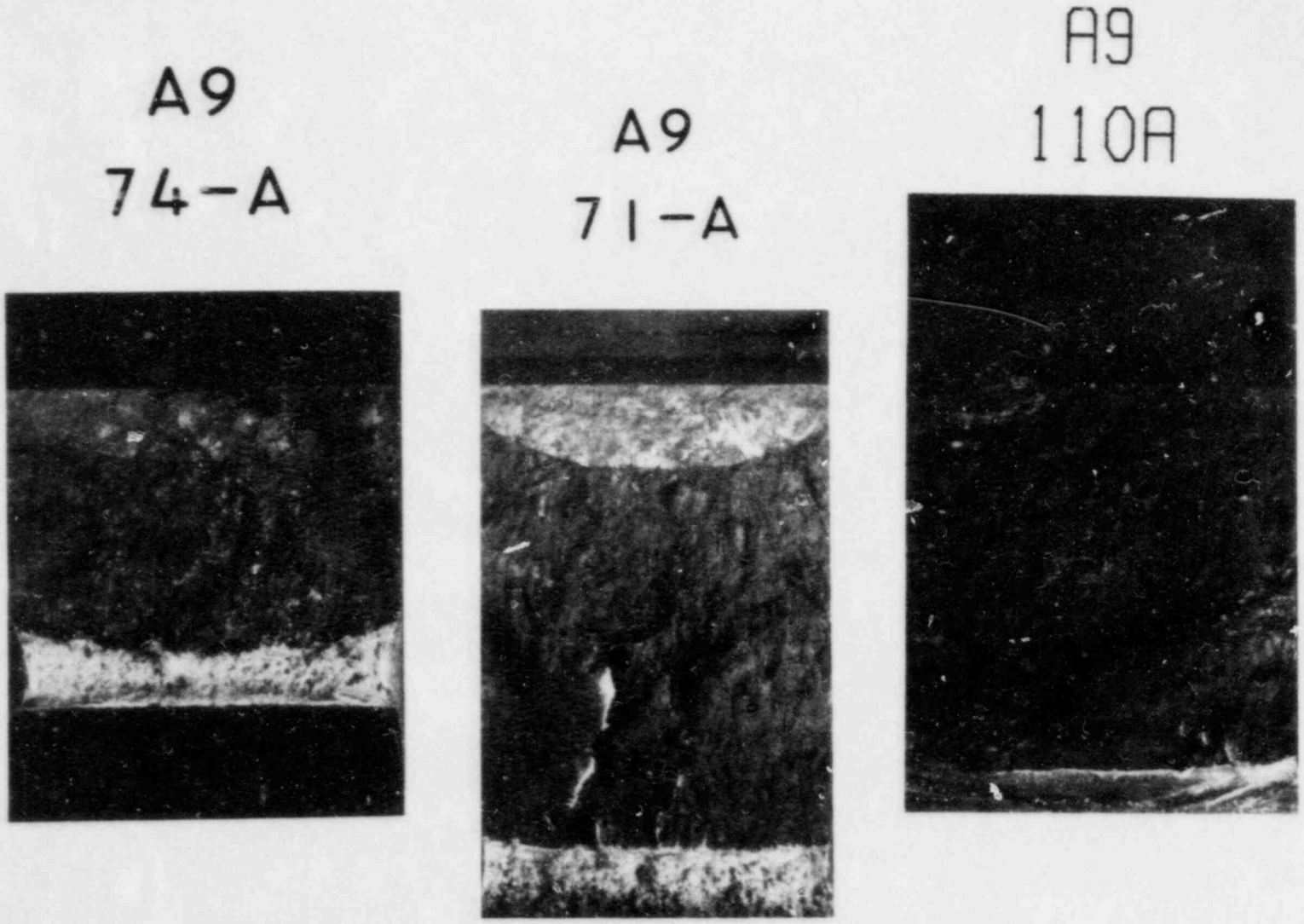

Fig. 12a. Macrophotographs of the specimens tested in the axial orientation for three temperatures, 232°C, 288°C and 338°C (450°F, 550°F and 640°F). The crack front tended to have a somewhat irregular profile for this orientation.

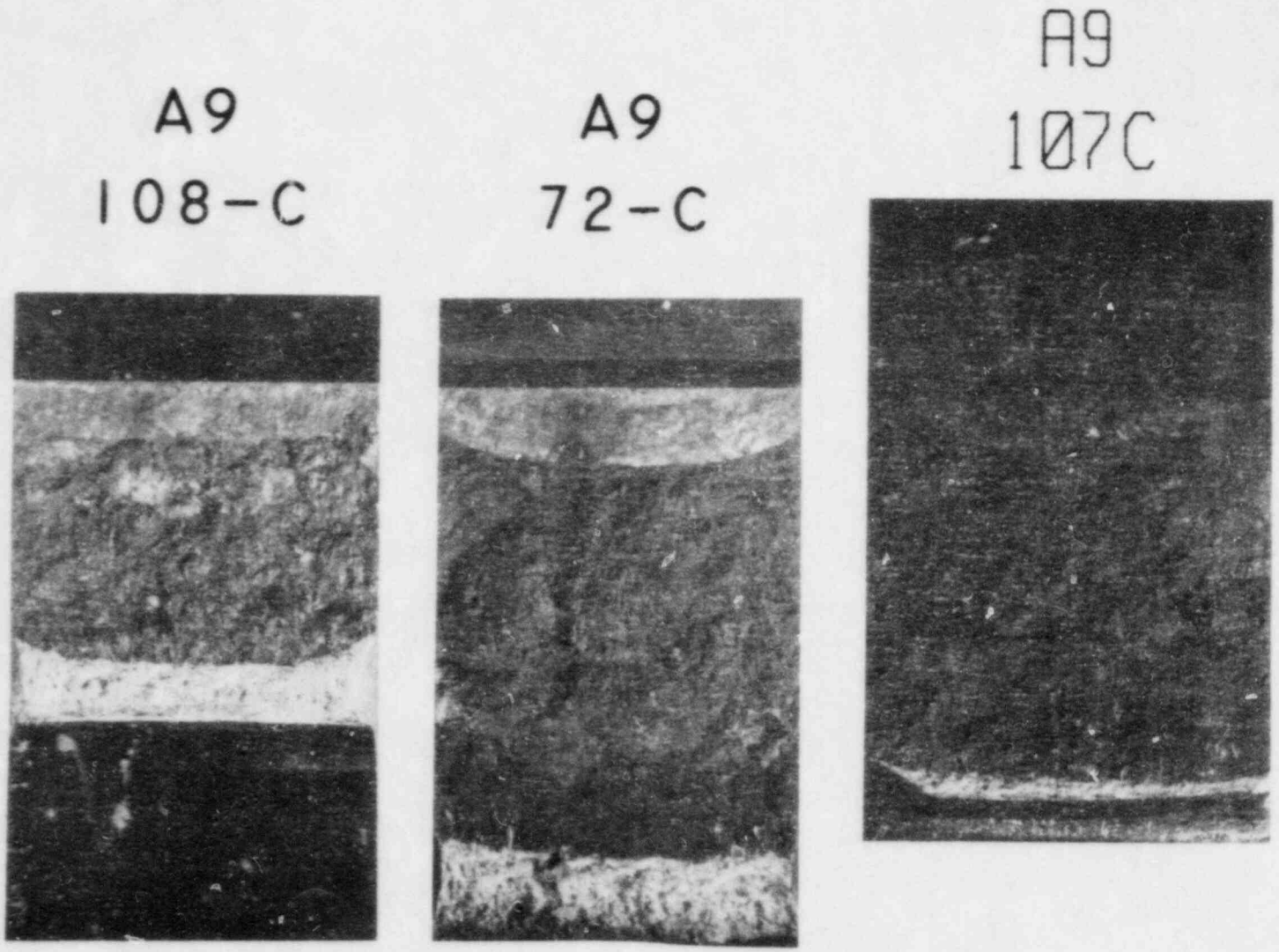

Fig. 12b. Macrophotographs of the specimens tested in the circumferential orientation for three temperatures, 232°C, 288°C and 338°C (450°F, 550°F and 640°F). The crack front is uniform, but quite deeply tunneled.

is sometimes scalloped, rather than smoothly convex. The fracture surface profiles shown in Fig. 13a and b indicate the way in which the fatigue crack propagates. In most cases the crack orients so that it cuts the Δ-ferrite phase at near-normal incidence. Secondary cracks are present at some of the austenite/Δ-ferrite interphase boundaries, but only on the edge met by the crack as it proceeds from austenite into Δ-ferrite.

Sets of SEM photographs from specimens tested at the three highest temperatures are shown in Figs. 14 to 22. These fractographs are arranged in groups of three for each specimen examined, showing three ΔK levels for each. The most distinctive feature is the very brittle-like appearance of the fatigue fracture surfaces. This characteristic pervades over all the temperatures, frequencies and ΔK levels tested, indicating that environmental effects influence strongly the cracking morphology, and hence the growth rates. There is no pitting evident, and the striations, where observed, are clear, well-defined and very regular. The striations appear in one of three forms. At low ΔK values, brittle-like striations are found on the fan-shaped features. At higher ΔK values, ductile striations are found on the fan-shaped features, and at the highest ΔK values, pure ductile-striated surfaces are seen. There is a slight increase in the amount of ductile-striated area on the specimens tested at the higher temperatures. A more complete analysis of the fractography is presented in Ref. 13.

Other observations can also be stated.

(a) The amount of ductile fatigue failure, in the form of striations and ductile tearing, increases with both increasing temperature and increasing ΔK.

(b) the brittle appearance bears a strong resemblance to the brittle characteristic observed in stress-corrosion cracking failures in stainless steels (Ref. 14).

(c) The brittle appearance occurs for both 1 Hz and 17 mHz test frequencies.

(d) Both ductile and brittle striations can be observed. In a few instances, cross-slip steps are visible.

(e) There is no connection between the inclusions and the advance of the fatigue crack, indicating that the inclusions play no role as centers for environmental degradation.

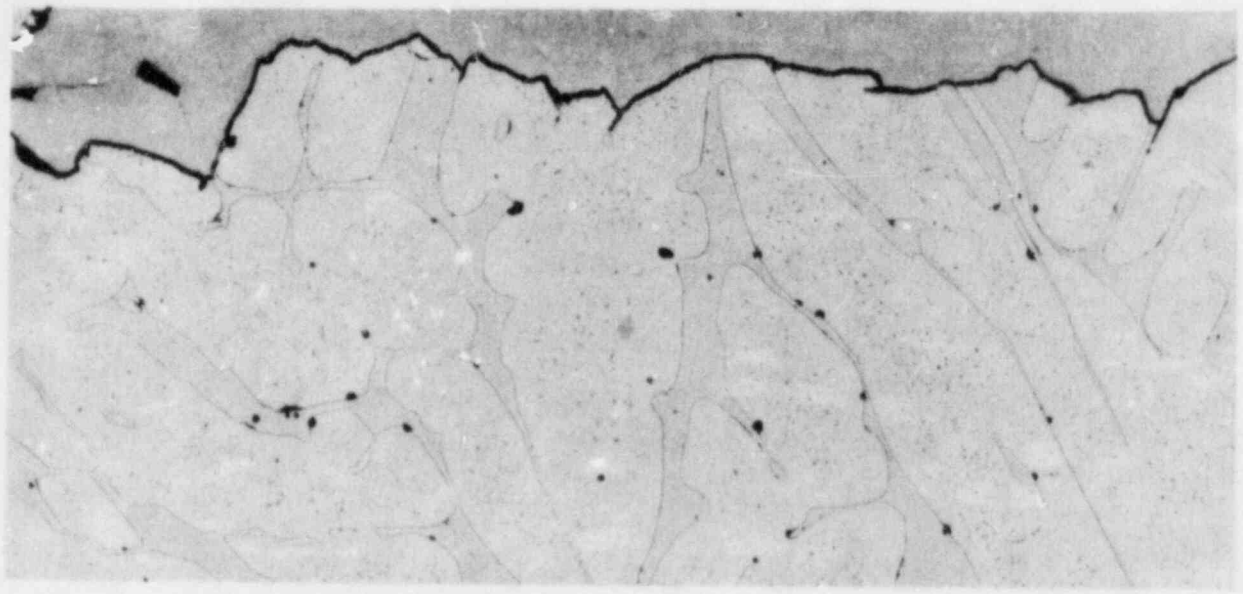

A

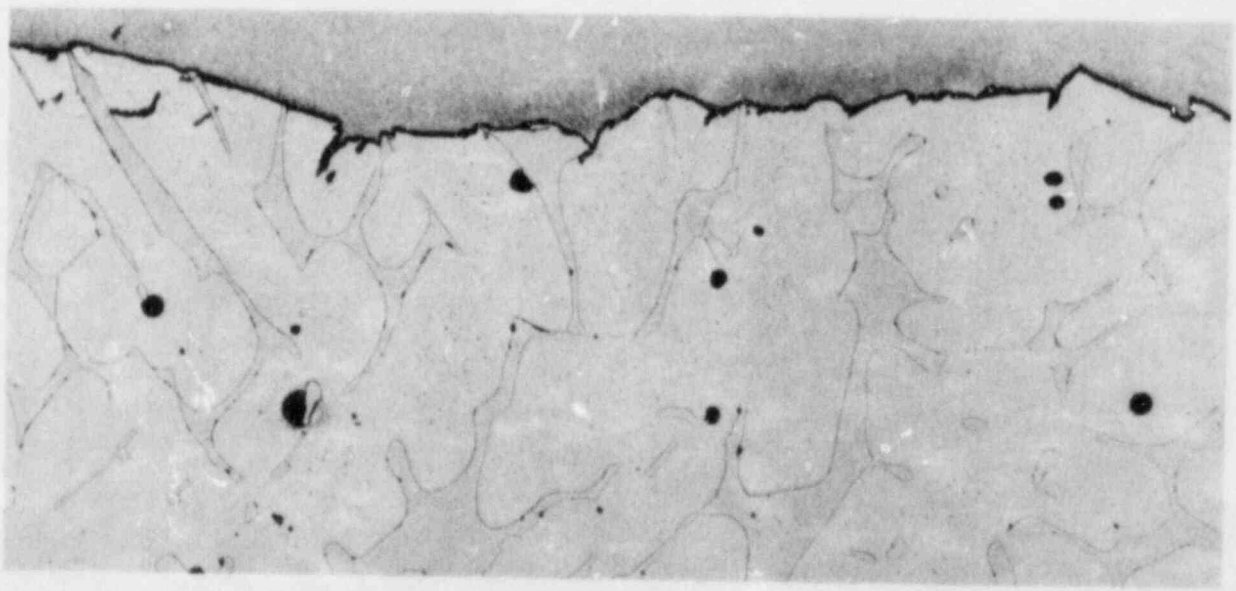

B

Fig. 13a and b. Fatigue fracture surface profiles showing the intergranular crack path and the influence of crystallographic orientation on the inclination and roughness of the fatigue crack.

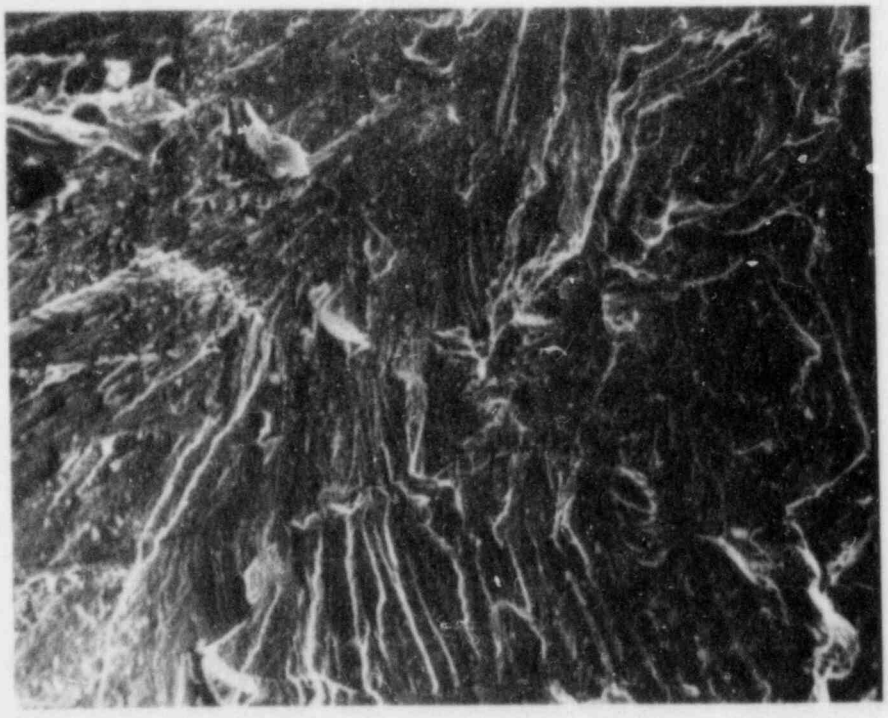

Fig. 14. Fatigue fracture surface of specimen A9-108C, tested at 232°C (450°F). Applied ΔK = 20 MPa$\sqrt{m}$. Note the clearly defined, brittle-like features, the microcracks along the interphase boundaries, and the embedded carbide particles, which play no role in the advance of the crack.

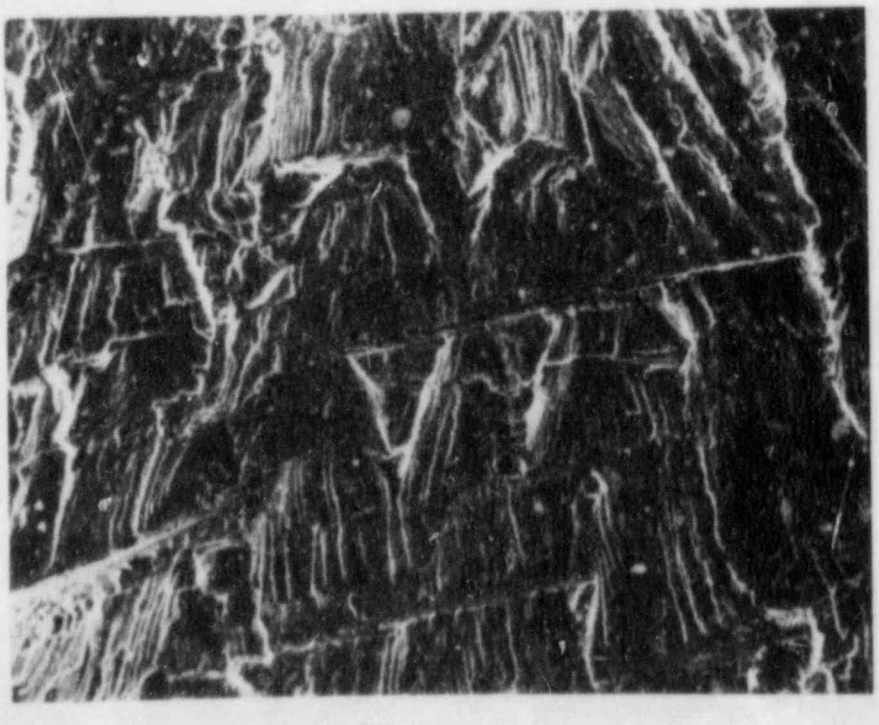

Fig. 15. Fatigue fracture surface of specimen A9-108C, tested at 232°C (450°F). Applied ΔK = 25 MPa$\sqrt{m}$. In this view, the brittle-like appearance is very clear.

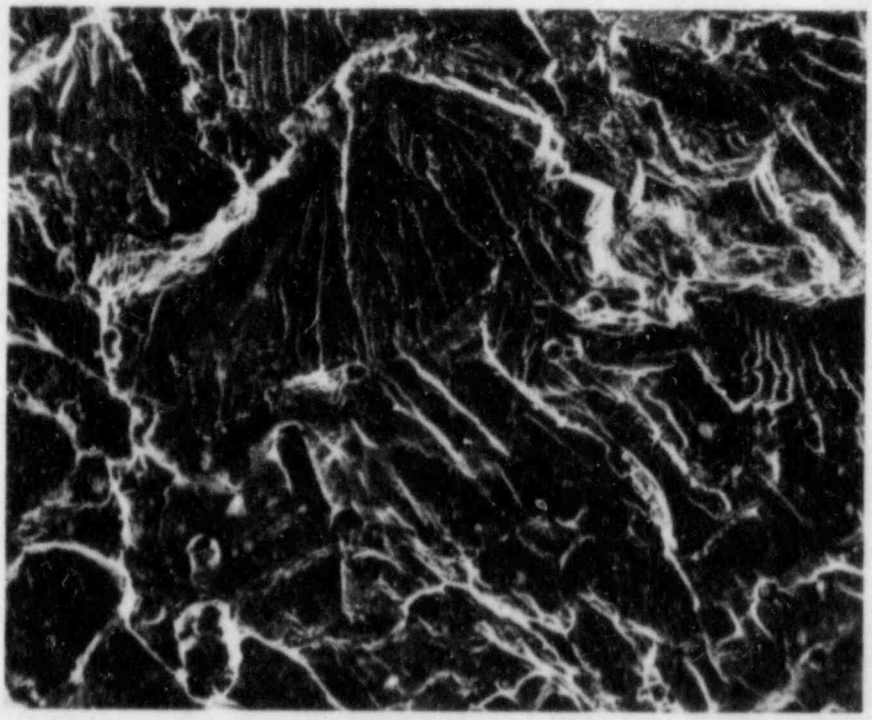

Fig. 16. Fatigue fracture surface of specimen A9-108C, tested at 232°C (450°F). Applied $\Delta K = 36$ MPa$\sqrt{m}$. The increased ductility resulting from the higher stress intensity factor, and higher growth rates is evident in this view.

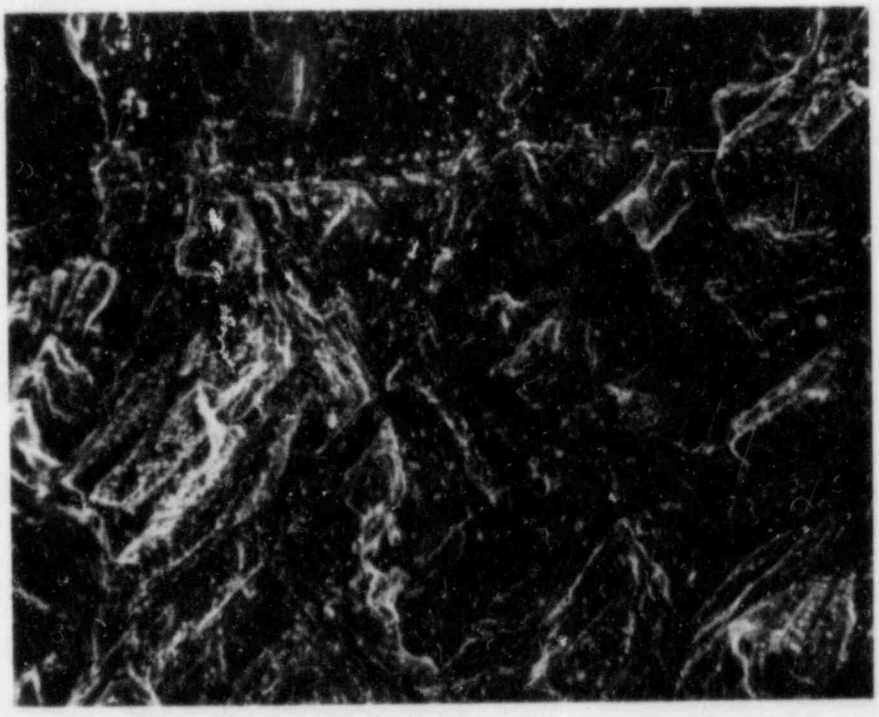

Fig. 17. Fatigue fracture surface of specimen A9-72, tested at 288°C (550°F). Applied $\Delta K = 18$ MPa$\sqrt{m}$. This photo shows the boundary at the very start of the environmentally-assisted test. The surface at the top is due to a 20 Hz precracking phase in air at room temperature; toward the bottom is due to 1 Hz in the pressurized, high-temperature water. Note that the change in fracture surface characteristics is immediate.

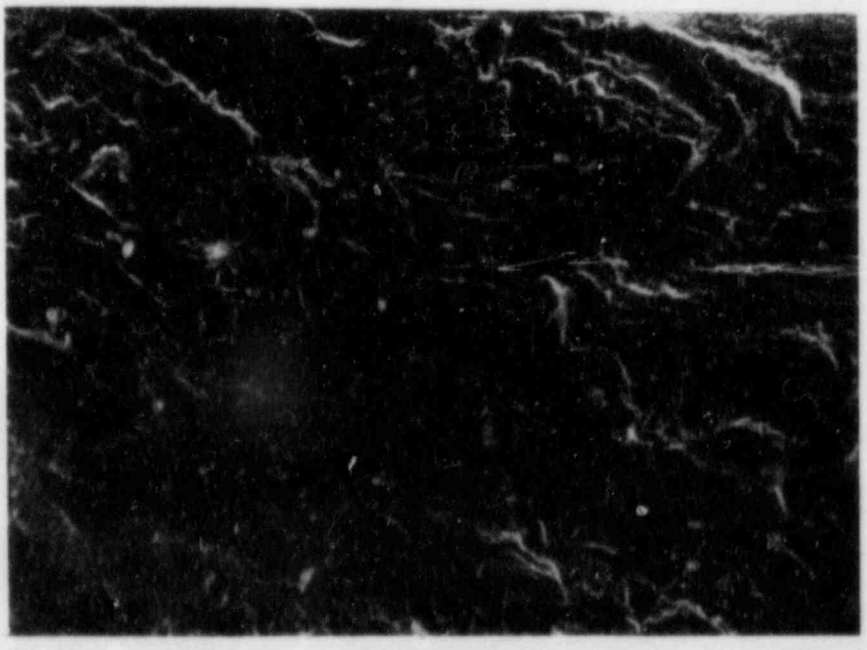

Fig. 18. Fatigue fracture surface of specimen A9-72C, tested at 288°C (550°F). Applied $\Delta K = 30$ MPa$\sqrt{m}$. The crack propagation is heavily influenced by the crystallography, but the amount of ductility is increased above that at the lower temperature.

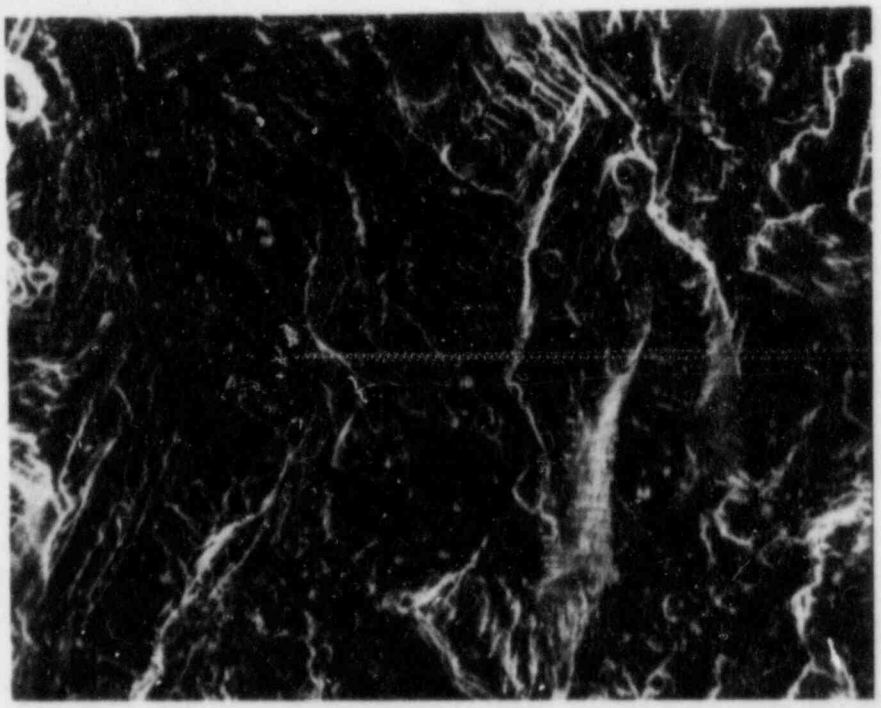

Fig. 19. Fatigue fracture surface of specimen A9-72C, tested at 288°C (550°F). Applied $\Delta K = 39$ MPa$\sqrt{m}$. Some ductile striations have formed on some of the transgranular fatigue fracture surface.

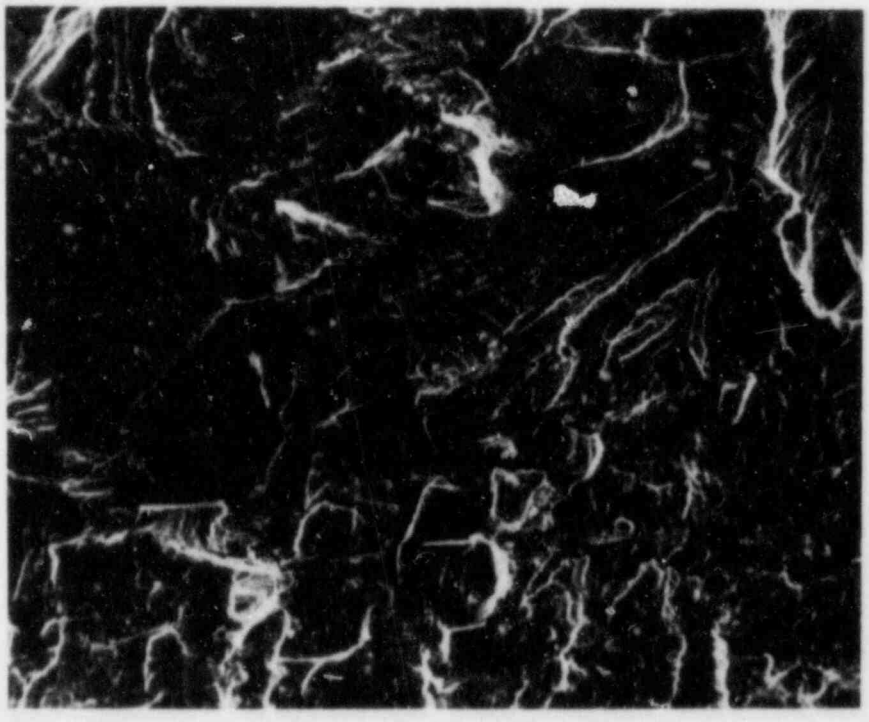

Fig. 20. Fatigue fracture surface of specimen A9-107C, tested at 338°C (640°F). Applied ΔK = 20 MPa$\sqrt{m}$. As the temperature increases the amount of the ductile fatigue component increases.

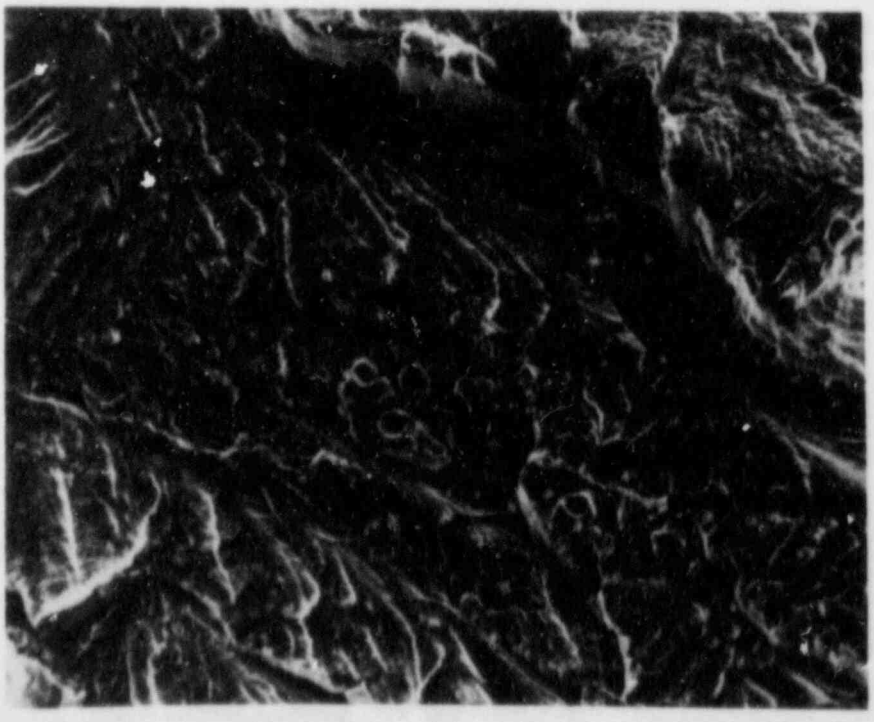

Fig. 21. Fatigue fracture surface of specimen A9-107C, tested at 338°C (640°F). Applied ΔK = 25 MPa$\sqrt{m}$. Ductile striations and embedded carbides are the important features in this photo.

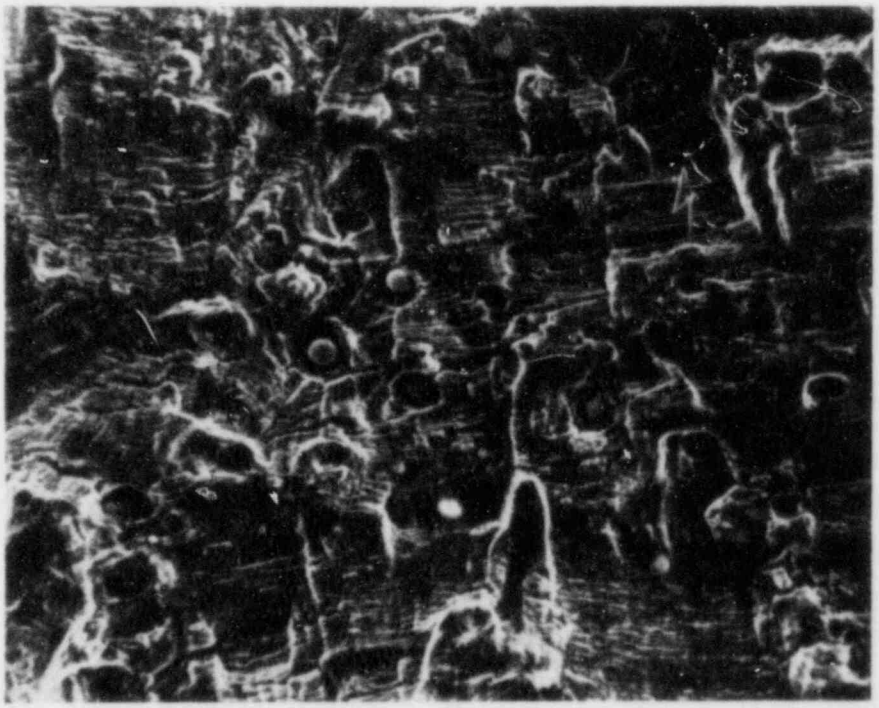

Fig. 22. Fatigue fracture surface of specimen A9-107C, tested at 388°C (640°F). Applied $\Delta K = 30$ MPa$\sqrt{m}$. At this temperature and applied ΔK level, the fatigue fracture surface is largely composed of ductile striations. Note that voids formed around the embedded particles, but that these do not influence the formation of the striations.

4. CONCLUSIONS

Consideration of the fatigue crack growth data and the supporting metallography and fractography leads to the following conclusions.

- There is an easily measurable, environmentally-induced increase in fatigue crack growth rates of cast stainless steels. The environmental effects are present at both 1 Hz and 17 mHz test frequencies, but growth rates are similar to those of low-alloy steels tested under similar conditions.

- There is little effect of temperature on the trend of the crack growth rates. The fracture surfaces show slightly increasing ductility with increasing temperature.

- The fractographic results indicate a highly brittle appearance of the fatigue fractures. Very clear striations are seen on some of the fan-shaped features. These can be either brittle-like in appearance, or very ductile-like. The ductile striations are frequent sites for secondary cracks. The amount of brittle-like striations decreases with increasing ΔK.

REFERENCES

1. W. H. Cullen, et al., "Operation of High-Temperature, Pressurized Water Fatigue Crack Growth System," Closed Loop Magazine, Oct. 1980, pp. 3-14.

2. Cullen, W. H. et al., "Fatigue Crack Growth of A 508-2 Steel in High-Temperature, Pressurized Reactor-Grade Water," USNRC Report NUREG/CR-0969, 1979.

3. W. H. Cullen, et al., "Fatigue Crack Growth Rates of Irradiated Pressure Vessel Steels in Simulated Nuclear Coolant Environment," Journal of Nuclear Materials, 96, 1981, pp. 261-268.

4. W. H. Cullen, B. H. Menke, H. E. Watson and F. J. Loss, "A Computerized Data Acquisition System for High-Temperature, Pressurized-Water, Fatigue Test Facility," in Computer Automation of Materials Testing, ASTM STP 710, American Society for Testing and Materials, 1980, pp. 127-140.

5. "Standard Test Method for Constant-Load-Amplitude Fatigue Crack Growth Rates Above 10^{-8} m/Cycle," Annual ASTM Standards, Part 10, Designation E647-78T. Issued annually.

6. L. A. James, "Fatigue-Crack Propagation in a Cast Stainless Steel," Nuclear Technology, 26 (1), 1975, pp. 46-53

7. W. H. Bamford, "Fatigue Crack Growth of Stainless Steel Piping in a Pressurized Water Reactor Environment," J. Pressure Vessel Tech., 101, 1979, pp. 73-79.

8. J. L. Bernard and G. S. Slama, "Fatigue Crack Growth Curve in Air Environment at 300°C for Stainless Steels," Nuclear Technology, 59, 1982, pp. 136-147.

9. C. Amzallag, G. Bauday, and J. L. Bernard, "Effects of PWR Environment on the Fatigue Crack Growth of Different Stainless Steels and Inconel-Type Alloys," in Proceedings of the International Atomic Energy Agency Specialists Meeting on Subcritical Crack Growth - Vol. 1, USNRC Conference Proceeding NUREG/CP-0044, 1983, pp. 163-194.

10. G. Slama, P. Petrequin and T. Mager, "Effect of Aging on Mechanical Properties of Austenitic Stainless Steel Castings and Welds," in Proceedings of Post-Conference Seminar #6, Assuring Structural Integrity of Steel Reactor Pressure Boundary Components, to be published (1983).

11. Section XI of the "ASME Boiler and Pressure Vessel Code, Rules for In-Service Inspection of Nuclear Power Plant Components ANSI/ASME-BPV-XI-1," American Society of Mechanical Engineers, New York. Issued annually.

12. W. H. Cullen, "Fatigue Crack Growth Rates of A 508-2 Steel in Pressurized, High-Temperature Water," USNRC Report NUREG/CR-3294, 1983.

13. W. H. Cullen, H. E. Hanninen, K. Torronen and M. Kemppainen, "The Temperature Dependence and Environmental Enhancement Mechanism of Fatigue Crack Growth Rates of A 351-CF8A Cast Stainless Steel in LWR Environment," in Proceedings of an IAEA Specialists' Meeting on Corrosion and Corrosion Fatigue in Steam Generators and Pressure Boundary Components, Technical Research Centre of Finland, Espoo, 1983.

14. H. E. Hanninen, "Influence of Metallurgical Variables on Environment-Sensitive Cracking of Austenitic Alloys," International Metals Reviews, Vol 24(3), 1979, pp. 85-135.

NRC FORM 335 (11-81)

U.S. NUCLEAR REGULATORY COMMISSION

BIBLIOGRAPHIC DATA SHEET

1. REPORT NUMBER *(Assigned by DDC)*
NUREG/CR-3546
MEA-2030

4. TITLE AND SUBTITLE *(Add Volume No., if appropriate)*
The Temperature Dependence of Fatigue Crack Growth Rates of A 351 CF8A Cast Stainless Steel in LWR Environment

2. *(Leave blank)*

3. RECIPIENT'S ACCESSION NO.

7. AUTHOR(S)
William H. Cullen, R. E. Taylor, K. Torronen, M. Kemppainen

5. DATE REPORT COMPLETED
MONTH: February | YEAR: 1984

9. PERFORMING ORGANIZATION NAME AND MAILING ADDRESS *(Include Zip Code)*
Materials Engineering Associates, Inc.
9700-B George Palmer Highway
Lanham, Maryland 20706

DATE REPORT ISSUED
MONTH: April | YEAR: 1984

6. *(Leave blank)*

8. *(Leave blank)*

12. SPONSORING ORGANIZATION NAME AND MAILING ADDRESS *(Include Zip Code)*
Division of Engineering Technology
Office of Nuclear Regulatory Research
U. S. Nuclear Regulatory Commission
Washington, D. C. 20555

10. PROJECT/TASK/WORK UNIT NO.

11. FIN NO.
B8133

13. TYPE OF REPORT
Technical Report

PERIOD COVERED *(Inclusive dates)*

15. SUPPLEMENTARY NOTES

14. *(Leave blank)*

16. ABSTRACT *(200 words or less)*

The fatigue crack growth rates for A 351-CF8A cast stainless steel were determined over a range of temperatures from 95°C to 338°C (200°F to 640°F). The waveform was 17 mHz sinusoidal and the load ratio was 0.2. The environment was borated and lithiated water with a dissolved oxygen content of ~ 1 ppb. The results show an easily measurable (factors of 2 to 8) increase in crack growth rates due to the environment. However, these rates are well within the known band of results for low-alloy pressure vessel and low-carbon piping steels in LWR environments. An extensive fractographic investigation shows fatigue fracture surfaces covered with brittle-like features. This morphology is similar to that resulting from the environmental assistance mechanism producing increased crack growth rates due to stress-corrosion cracking.

17. KEY WORDS AND DOCUMENT ANALYSIS

17a. DESCRIPTORS

Fatigue crack growth
Piping steels
Stainless steels
Fractography
Environmental effects
A 351-CF8A steel
Temperature effects

17b. IDENTIFIERS/OPEN-ENDED TERMS

18. AVAILABILITY STATEMENT
Unlimited

19. SECURITY CLASS *(This report)*
Unclassified

21. NO. OF PAGES

20. SECURITY CLASS *(This page)*
Unclassified

22. PRICE
$

NRC FORM 335 (11-81)

NUREG/CR-3546

THE TEMPERATURE DEPENDENCE OF FATIGUE CRACK GROWTH RATES OF A 351 CF8A CAST STAINLESS STEEL IN LWR ENVIRONMENT

APRIL 1984